

# A concept of polymeric networks with sliding junctions for the time-dependent response of filled elastomers

Aleksey D. Drozdov and Al Dorfmann  
Institute of Structural Engineering  
82 Peter Jordan Street  
A-1190 Vienna, Austria

## Abstract

Constitutive equations are derived for the time-dependent behavior of particle-reinforced elastomers at isothermal loading with finite strains. A rubbery polymer is modelled as a network of macromolecules bridged by junctions which can slip with respect to the bulk material under straining. A filled elastomer is thought of as an ensemble of meso-regions where sliding occurs with different rates. Stress-strain relations for a particle-reinforced rubber are developed by using the laws of thermodynamics. For tensile relaxation tests, these equations are characterized by three adjustable parameters. To determine the experimental constants, three series of relaxation tests are performed for longitudinal strains in the range from 100 to 250 %. By fitting observations, the influence of pre-loading and thermal recovery is analyzed on the nonlinear viscoelastic response of natural rubber reinforced with carbon black.

**Key-words:** Filled elastomers, Viscoelasticity, Finite strains, Polymeric networks, Constitutive equations

# 1 Introduction

This paper is concerned with modelling the time-dependent behavior of particle-reinforced elastomers at isothermal loading with finite strains. The viscoelastic and viscoplastic responses of filled rubbers have been a focus of attention in the past decade, which may be explained by numerous applications of rubber-like materials in industry (vehicle tires, shock absorbers, earthquake bearings, seals, flexible joints, solid propellants, etc.), see, e.g., Govendjee and Simo (1992), Johnson and Stacer (1993), Häusler and Sayir (1995), Johnson et al. (1995), Aksel and Hübner (1996), Holzapfel and Simo (1996), Lion (1996, 1997, 1998), Spathis (1997), Bergström and Boyce (1998), Ha and Schapery (1998), Reese and Govindjee (1998), Septanika and Ernst (1998), Miehe and Keck (2000), Wu and Liechti (2000), Haupt and Sedlan (2001), to mention a few. Despite numerous publications on this subject, some important issues remain, however, obscure.

One of the basic questions to be resolved deals with the physical nature of the time-dependent response of rubber-like materials at the micro-level. There is no agreement in the literature about the micro-mechanisms for stress relaxation in unfilled elastomers.

The relaxation process is conventionally modelled within the concept of temporary networks (Green and Tobolsky, 1946). A rubbery polymer is treated as a network of macromolecules bridged by junctions (chemical and physical cross-links, entanglements and van der Waals forces). With reference to the affinity hypothesis, junctions are assumed to be rigidly connected with the bulk material, whereas the time-dependent behavior of rubber is associated with breakage of active strands (whose ends are linked to separate junctions) and reformation of dangling strands (where stresses totally relax before these chains merge with the network).

Another scenario for the stress relaxation in rubbery polymers is based on the model of non-affine junctions which presumes that the network of macromolecules is permanent, whereas the time-dependent behavior at the macro-level reflects slippage of junctions with respect to the bulk medium at the micro-level. This approach was first suggested for polymeric melts by Phan-Thien and Tanner (1977) and Phan-Thien (1978) and was applied to filled elastomers by Desmorat and Cantournet (2001).

A version of the concept of non-affine networks, where junctions do not slip with respect to the bulk medium, but polymeric chains slide with respect to entanglements was proposed by Miehe and co-authors for the numerical analysis of stresses in rubbery vulcanizates (Miehe, 1995; Miehe and Keck, 2000, Lulei and Miehe, 2001). A similar model (where chains slip with respect to filler particles instead of entanglements) was recently introduced by Hansen (2000) based on results of molecular dynamics simulations and atomic force microscopy measurements.

The above theories concentrate on relatively slow relaxation processes when stresses relax at the time-scale corresponding to structural changes for the entire macromolecule. A fast relaxation (whose characteristic time is associated with the time for rearrangement of a mechanical segment in a chain) was studied by Drozdov (2001) by using a micro-mechanical scenario for relaxation in rubbery polymers similar to the tube model for concentrated polymeric solutions and melts (Doi and Edwards, 1986). The difference between the two approaches is that the conventional tube theory is based on the reptation concept for polymeric chains (this kind of diffusive motion is prevented by junctions in

cross-linked elastomers), whereas the concept of wavy tubes ascribes the time-dependent response of rubbers at the macro-level to mechanically induced changes in the concentration of regions with high molecular mobility in an individual strand at the micro-level. A transition mechanism from the stress relaxation at the length-scale of statistical segments to that at the length-scale of a chain in a polymer melt was recently discussed by Herman (2001).

This brief list of basic concepts in finite viscoelasticity and viscoplasticity of rubber-like materials evidences that our knowledge of micro-mechanisms for the time-dependent response of unfilled rubbers is far away from being exhausted. The physics of the viscoelastic and viscoplastic behavior of particle-reinforced elastomers remains rather obscure, which implies that a number of different micro-mechanical theories are proposed to describe stress relaxation in filled rubbers.

On the one hand, Aksel and Hübner (1996), Kaliske and Rothert (1998) and Hansen (2000) explained the time-dependent response of particle-reinforced rubbers by sliding of polymeric chains along and their de-wetting from the surfaces of filler clusters. This concept goes back to the model proposed by Dannenberg (1975), which, in turn, is equivalent to the assumption that the ability of a host matrix to relax is negligible, the hypothesis suggested about half a century ago by Bueche (1960, 1961) to explain the Mullins effect.

On the other hand, Liang et al. (1999), Clarke et al. (2000) and Leblanc and Cartault (2001) evidenced that the effect of particles and their aggregates on the viscoelastic response of rubbery compounds is not crucial. Leblanc and Cartault (2001) performed dynamic shear tests on uncured styrene-butadiene rubber reinforced with various amounts of carbon black and silica and revealed that the compounds exhibited rather limited time-dependent response. These observations allowed them to infer that interactions between chains (cross-links) play the key role in the viscoelastic behavior, whereas the influence of filler is of second importance. Liang et al. (1999) reported experimental data in dynamic tensile tests on ternary composite of polypropylene and EPDM (ethylene propylene diene monomers) elastomer filled with glass beads. They demonstrated that treatment of beads by silane coupling agent did not affect mechanical damping and that the loss modulus of the compound with untreated beads decreased with the concentration of filler (in contrast with the de-wetting concept). Clarke et al. (2000) carried out tensile relaxation tests on two unfilled elastomers (natural polyisoprene rubber and synthetic polyacrylate rubber) at the temperature  $T = 80$  °C and found significant relaxation of stresses in natural rubber, whereas no relaxation was revealed in the synthetic elastomer.

Our experimental data in tensile relaxation tests on natural rubber reinforced with high abrasion furnace black demonstrated comparable decreases in the longitudinal stress for a filled [45 phr (parts per hundred parts of rubber) of carbon black (CB)] and an unfilled [1 phr of CB] compounds (Drozdov and Dorfmann, 2001). Because the amount of stress relaxed during 1 hour at ambient temperature in the CB filled specimens exceeded (approximately by a factor of 2) that for the unfilled samples, we suppose that a physical mechanism for relaxation of stresses is in between the above two extreme concepts: the relaxation process in particle-reinforced rubbery polymers may be associated with rearrangement of macromolecules in the matrix, but the rearrangement process is strongly affected by local inhomogeneities induced by the presence of filler.

In accord with this picture, we model a filled rubber as a network of macromolecules

bridged by junctions. To account for the effect of filler particles and their agglomerates on the time-dependent response of the network in a tractable way, the network is treated as an ensemble of meso-domains, where rearrangement of strands occurs with different (mutually independent) rates. The characteristic size of these regions is assumed to substantially exceed the radius of gyration for macromolecules and the mean radius of particles, on the one hand, and to be noticeably less than the dimensions of a macro-specimen. The characteristic length of a meso-domain is roughly estimated as several hundreds of nm. The ensemble of meso-domains reflects local inhomogeneities in the rubber-like material caused by impurities, non-homogeneity in the spatial distribution of a cross-linker and a filler, local fluctuations of elastic moduli associated with the presence of hard cores around filler clusters (Karasek and Sumita, 1996), as well as the enhancement of the rearrangement process for strands bridged to aggregates of filler (Karasek and Sumita, 1996).

With reference to the concept of sliding junctions, different meso-regions are characterized by different potential energies,  $\omega$ , for slippage of junctions with respect to the bulk material. The rate of slippage,  $\Gamma$ , is expressed in terms of the potential energy,  $\omega$ , by the Boltzmann formula. This implies that rearrangement of strands in a particle-reinforced elastomer is entirely determined by the attempt rate,  $\Gamma_0$ , and the distribution function,  $p(\omega)$ , of potential energies for sliding.

To account for the effect of strain intensity on the rate of stress relaxation, we distinguish between active meso-domains, where junctions can freely slide, and passive meso-regions, where sliding is prevented by surrounding macromolecules (because the local concentration of cross-links in these domains exceeds the average one). Under stretching, some van der Waals links between strands break in passive meso-domains, which implies that these regions are transformed into the active state. The ability of a passive meso-region to become active is determined by a measure of damage,  $\alpha$ , which characterizes the relative number of extra links between polymeric chains which do not allow the sliding process to start. The present study focuses on active loading programs in which passive meso-regions are transformed into the active state when the stress intensity grows. Healing of links between chains resulting in the inverse transformation at unloading remains beyond the scope of this work.

The objective of this paper is three-fold:

1. To develop constitutive equations for the time-dependent response of a particle-reinforced elastomer modelled as an ensemble of meso-regions with various potential energies for sliding. We confine ourselves to filled rubbers with the volume fractions of particles,  $\varphi$ , below the percolation threshold, which implies that nano-clusters of filler are not aggregated into an infinite secondary network.
2. To expose experimental data in three series of tensile relaxation tests on CB filled natural rubber at various longitudinal strains in the range from 100 to 250 %. The first series of tests was carried out on virgin specimens, in the second series the samples were initially pre-loaded, whereas the third series dealt with the same specimens after thermal recovery at an elevated temperature.
3. To find adjustable parameters by fitting observations and to rationalize the influence

of pre-loading and thermal recovery on the nonlinear viscoelastic behavior of filled elastomers in terms of the constitutive model.

The study is organized as follows. Sliding of junctions in active meso-regions and transition of passive meso-domains into the active state are discussed in Section 2. Kinematic equations for slippage of junctions with respect to the bulk medium are developed in Section 3. The strain energy density of a particle-reinforced elastomer is determined in Section 4. Stress–strain relations are derived in Section 5 by using the laws of thermodynamics. Uniaxial extension of a specimen is analyzed in Section 6. Section 7 deals with the description of the experimental procedure. Adjustable parameters in the constitutive equations are determined by fitting observations in Section 8, where some physical interpretation is provided for our findings. Some concluding remarks are formulated in Section 9.

## 2 Deformation of a particle-reinforced elastomer

A filled rubber is thought of as a highly inhomogeneous medium at the meso-scale. A particle-reinforced elastomer is modelled as an ensemble of meso-domains (with arbitrary shapes) where junctions can slip with respect to the bulk material. Sliding of junctions is assumed to occur independently in different meso-regions.

A meso-domain is characterized by its potential energy  $\omega$ , which is defined as follows. Slippage of junctions with respect to their positions in the bulk material is thought of as a viscous flow with the constitutive equation

$$\sigma = \eta \dot{\epsilon}, \quad (1)$$

where  $\sigma$  is the stress,  $\dot{\epsilon}$  is the strain rate, and  $\eta > 0$  is some viscosity. The parameter  $\eta$  in Eq. (1) is given by

$$\eta = \frac{G}{\Gamma}, \quad (2)$$

where  $G$  stands for an elastic modulus, and  $\Gamma$  is the rate of sliding. For definiteness, we suppose that  $G$  coincides for all meso-domains, whereas  $\Gamma$  accepts different values for different regions. The Boltzmann formula is adopted for the rate of sliding

$$\Gamma = \Gamma_0 \exp\left(-\frac{\bar{\omega}}{k_B T}\right), \quad (3)$$

where  $\bar{\omega}$  is the potential energy of a meso-region,  $T$  is the absolute temperature,  $k_B$  is Boltzmann's constant, and the pre-factor  $\Gamma_0$  weakly depends on temperature. The attempt rate  $\Gamma_0$  equals the rate of sliding for junctions at an elevated temperature ( $T \rightarrow \infty$ ). Introducing the dimensionless potential energy,

$$\omega = \frac{\bar{\omega}}{k_B T_0},$$

where  $T_0$  is some reference temperature, and disregarding the effect of small temperature increments,  $\Delta T = T - T_0$ , on the sliding process, we find from Eq. (3) that

$$\Gamma = \Gamma_0 \exp(-\omega). \quad (4)$$

Equation (4) expresses the rate of slippage of junctions with respect to the bulk medium,  $\Gamma$ , in a meso-region in terms of its potential energy,  $\omega$ .

The potential energy  $\omega$  characterizes the rate of sliding of junctions in a meso-domain provided that the sliding process is not affected by mutual interaction of strands. In other words, this quantity determines the rate of sliding in a *hypothetical* meso-region where all inter-chain interactions are disregarded (the neglect of interactions between strands is a conventional hypothesis in the entropic theory of rubber elasticity, where the number of available configurations for a chain is determined under the assumption that surrounding macromolecules do not restrict the chain geometry). For a *real* elastomer, the neglect of interaction between polymeric chains may be accepted only for a part of the ensemble of meso-domains. In other meso-regions interactions between chains prevent sliding of junctions until micro-strains become sufficiently large to break inter-chain links (which reflect van der Waals' forces between strands) that do not allow the sliding process to start.

With reference to this picture, all meso-domains in an ensemble are divided into two groups:

- active regions where sliding of junctions is unrestricted,
- passive domains where slippage of junctions is inhibited by inter-chain interactions.

The sliding process in an active meso-region is entirely described by its potential energy,  $\omega$ . To characterize the ability of a passive meso-domain to be transformed into an active one, we introduce an additional variable,  $\alpha$ , which is treated a measure of damage for inter-chain interactions driven by mechanical factors.

Any interaction between polymeric chains that prevents slippage of junctions with respect to the bulk material may be thought of as a temporary link between macromolecules. Mechanically-induced weakening of interactions between strands is modelled as rupture of temporary links under loading.

We suppose that the number of meso-regions with potential energy  $\omega$  per unit mass of an elastomer is rather large, denote by  $\langle M(\omega) \rangle$  the average number of inter-chain links per unit domain before loading, and by  $M(t, \omega)$  the number of these links in a meso-domain in the deformed state at time  $t$  (the initial instant  $t = 0$  corresponds to the time when external forces are applied to a specimen). The measure of damage,  $\alpha$ , is defined as the ratio of these quantities,

$$\alpha(t, \omega) = \frac{M(t, \omega)}{\langle M(\omega) \rangle}. \quad (5)$$

Unlike the standard approach in the fracture theory, where the initial measure of damage is assumed to vanish, whereas fracture of a macro-sample is associated with some positive value of the damage variable (conventionally, unity), Eq. (5) implies that for a stress-free state of an elastomer,  $\alpha$  is positive, and it equals zero when a passive meso-region is transformed into an active one.

It follows from Eq. (5) that the initial value of the damage variable,  $\alpha$ , may be either higher or lower than 1 in various meso-domains, whereas the average value of  $\alpha(0, \omega)$  equals unity. The condition  $\alpha(0, \omega) < 1$  means that a passive meso-domain is initially

damaged. This damage is associated with breakage of inter-chain interactions in meso-domains during the preparation process (at the stage of milling of a rubbery compound). On the other hand, the inequality  $\alpha(0, \omega) > 1$  implies that the number of links between macromolecules in a passive meso-domain in a virgin specimen exceeds its average value, which may be ascribed to local inhomogeneities in the distribution of a cross-linker.

In accord with this picture, the distribution of passive meso-domains is described by the function  $\Xi_p(t, \alpha, \omega)$  which equals the current number of passive meso-regions (per unit mass) with the potential energy  $\omega$  where the damage variable equals  $\alpha$ . Summing the number of meso-domains with various measures of damage,  $\alpha$ , we find the concentration of passive regions with potential energy  $\omega$ ,

$$X_p(t, \omega) = \int_0^\infty \Xi_p(t, \alpha, \omega) d\alpha. \quad (6)$$

The number of passive regions per unit mass,  $N_p$ , equals the sum of the numbers of passive meso-domains with various potential energies,  $\omega$ ,

$$N_p(t) = \int_0^\infty X_p(t, \omega) d\omega. \quad (7)$$

Denote by  $X_a(t, \omega)$  the current number of active meso-domains with potential energy  $\omega$ . The quantities  $X_a$  and  $X_p$  are connected by the conservation law

$$X_a(t, \omega) + X_p(t, \omega) = X(\omega), \quad (8)$$

where  $X(\omega)$  is the concentration of meso-regions with potential energy  $\omega$ . Differentiation of Eq. (8) with respect to time implies that

$$\gamma(t, \omega) = \frac{\partial X_a}{\partial t}(t, \omega) = -\frac{\partial X_p}{\partial t}(t, \omega), \quad (9)$$

where  $\gamma(t, \omega)$  is the rate of transformation of passive meso-domains into active ones. Integrating Eq. (8) over  $\omega$  and using Eq. (7), we find that

$$N_a(t) + N_p(t) = N, \quad (10)$$

where

$$N_a(t) = \int_0^\infty X_a(t, \omega) d\omega \quad (11)$$

is the current concentration of active meso-domains and

$$N = \int_0^\infty X(\omega) d\omega$$

is the total number of meso-regions per unit mass.

### 3 Kinematic relations

Let  $\mathbf{r}_0$  be the radius vector of an arbitrary junction in the reference state,  $\mathbf{r}(t, \mathbf{r}_0)$  its radius vector in the deformed state at time  $t$ , and  $\mathbf{r}_u(t, \mathbf{r}_0)$  the radius vector of this point in the

unloaded state. In what follows, the argument  $\mathbf{r}_0$  of the functions  $\mathbf{r}$  and  $\mathbf{r}_u$  is omitted for the sake of simplicity.

The unloaded state of a meso-region is determined by the positions which junctions accept at time  $t$  because of their slippage with respect to the initial configuration. The displacement vector for transition of a junction from its reference state to the unloaded state is given by

$$\mathbf{u}_u(t) = \mathbf{r}_u(t) - \mathbf{r}_0.$$

Denote by  $\nabla_0\mathbf{r}(t)$  the deformation gradient for transition from the reference state to the actual state, by  $\nabla_0\mathbf{r}_u(t)$  the deformation gradient for transition from the reference state to the unloaded state, and by  $\nabla_u(t)\mathbf{r}(t)$  the deformation gradient for transition from the unloaded state to the deformed state. Here  $\nabla_0$  and  $\nabla_u(t)$  are the gradient operators in the initial and unloaded configurations, respectively. With reference to Drozdov (1996), the “left” gradient operators are employed, which means that the image,  $d\mathbf{r}(t)$ , in the actual state of an infinitesimal vector,  $d\mathbf{r}_0$ , in the reference state reads

$$d\mathbf{r}(t) = d\mathbf{r}_0 \cdot \nabla_0\mathbf{r}(t),$$

where the dot stands for inner product. The deformation gradients are connected by the equation

$$\nabla_0\mathbf{r}(t) = \nabla_0\mathbf{r}_u(t) \cdot \nabla_u(t)\mathbf{r}(t), \quad (12)$$

which expresses the chain rule for differentiation of the vector function  $\mathbf{r} = \mathbf{r}(t, \mathbf{r}_0)$  with respect to  $\mathbf{r}_0$ .

The right Cauchy deformation tensor,  $\mathbf{C}(t)$ , for transition from the initial state to the deformed state is determined by the formula

$$\mathbf{C}(t) = \nabla_0\mathbf{r}(t) \cdot [\nabla_0\mathbf{r}(t)]^\top, \quad (13)$$

where  $\top$  denotes transpose. By analogy with Eq. (13), we introduce the right Cauchy deformation tensor for transition from the reference state to the unloaded state,

$$\mathbf{C}_u(t) = \nabla_0\mathbf{r}_u(t) \cdot [\nabla_0\mathbf{r}_u(t)]^\top, \quad (14)$$

and the right Cauchy deformation tensor for transition from the unloaded state to the actual state,

$$\mathbf{C}_e(t) = \nabla_u(t)\mathbf{r}(t) \cdot [\nabla_u(t)\mathbf{r}(t)]^\top. \quad (15)$$

It follows from Eqs. (12), (13) and (15) that

$$\begin{aligned} \mathbf{C}_e(t) &= [\nabla_0\mathbf{r}_u(t)]^{-1} \cdot \nabla_0\mathbf{r}(t) \cdot [\nabla_0\mathbf{r}(t)]^\top \cdot [\nabla_0\mathbf{r}_u(t)]^{-\top} \\ &= [\nabla_0\mathbf{r}_u(t)]^{-1} \cdot \mathbf{C}(t) \cdot [\nabla_0\mathbf{r}_u(t)]^{-\top}. \end{aligned} \quad (16)$$

The left Cauchy deformation tensor for transition from the reference state to the deformed state reads

$$\mathbf{B}(t) = [\nabla_0\mathbf{r}(t)]^\top \cdot \nabla_0\mathbf{r}(t), \quad (17)$$

whereas the left Cauchy deformation tensor for transition from the unloaded state to the actual state is given by

$$\mathbf{B}_e(t) = [\nabla_{\mathbf{u}}(t)\mathbf{r}(t)]^\top \cdot \nabla_{\mathbf{u}}(t)\mathbf{r}(t). \quad (18)$$

Equations (12), (14) and (18) imply that

$$\begin{aligned} \mathbf{B}_e(t) &= [\nabla_0\mathbf{r}(t)]^\top \cdot [\nabla_0\mathbf{r}_u(t)]^{-\top} \cdot [\nabla_0\mathbf{r}_u(t)]^{-1} \cdot \nabla_0\mathbf{r}(t) \\ &= [\nabla_0\mathbf{r}(t)]^\top \cdot \mathbf{C}_u^{-1}(t) \cdot \nabla_0\mathbf{r}(t). \end{aligned} \quad (19)$$

Our purpose now is to determine the derivatives of the principal invariants,  $I_k$  ( $k = 1, 2$ ), of the tensor  $\mathbf{C}_e(t)$  with respect to time. Differentiation of Eq. (15) results in

$$\begin{aligned} \frac{d\mathbf{C}_e}{dt}(t) &= \frac{d}{dt}[\nabla_0\mathbf{r}_u(t)]^{-1} \cdot \mathbf{C}(t) \cdot [\nabla_0\mathbf{r}_u(t)]^{-\top} \\ &\quad + [\nabla_0\mathbf{r}_u(t)]^{-1} \cdot \frac{d\mathbf{C}}{dt}(t) \cdot [\nabla_0\mathbf{r}_u(t)]^{-\top} \\ &\quad + [\nabla_0\mathbf{r}_u(t)]^{-1} \cdot \mathbf{C}(t) \cdot \frac{d}{dt}[\nabla_0\mathbf{r}_u(t)]^{-\top}. \end{aligned} \quad (20)$$

Bearing in mind that

$$\frac{d\mathbf{r}_u}{dt}(t) = \mathbf{v}_u(t),$$

where  $\mathbf{v}_u(t)$  is the velocity vector for sliding of junctions, and using the chain rule for differentiation, we obtain

$$\frac{d}{dt}[\nabla_0\mathbf{r}_u(t)] = \nabla_0\mathbf{v}_u(t) = \nabla_0\mathbf{r}_u(t) \cdot \mathbf{L}_u(t), \quad (21)$$

where

$$\mathbf{L}_u(t) = \nabla_{\mathbf{u}}(t)\mathbf{v}_u(t).$$

Taking into account that

$$\frac{d}{dt}[\nabla_0\mathbf{r}_u(t)]^{-1} = -[\nabla_0\mathbf{r}_u(t)]^{-1} \cdot \frac{d}{dt}[\nabla_0\mathbf{r}_u(t)] \cdot [\nabla_0\mathbf{r}_u(t)]^{-1},$$

we find from Eq. (21) that

$$\frac{d}{dt}[\nabla_0\mathbf{r}_u(t)]^{-1} = -\mathbf{L}_u(t) \cdot [\nabla_0\mathbf{r}_u(t)]^{-1}. \quad (22)$$

It follows from Eq. (13) that the derivative of the Cauchy deformation tensor  $\mathbf{C}(t)$  reads

$$\frac{d\mathbf{C}}{dt}(t) = \nabla_0\mathbf{v}(t) \cdot [\nabla_0\mathbf{r}(t)]^\top + \nabla_0\mathbf{r}(t) \cdot [\nabla_0\mathbf{v}(t)]^\top, \quad (23)$$

where

$$\mathbf{v}(t) = \frac{d\mathbf{r}}{dt}(t)$$

is the velocity vector. Taking into account that

$$\nabla_0 \mathbf{v}(t) = \nabla_0 \mathbf{r}(t) \cdot \nabla(t) \mathbf{v}(t),$$

where  $\nabla(t)$  is the gradient operator in the deformed configuration, and setting

$$\mathbf{L}(t) = \nabla(t) \mathbf{v}(t),$$

we arrive at the formula

$$\frac{d\mathbf{C}}{dt}(t) = \nabla_0 \mathbf{r}(t) \cdot \mathbf{L}(t) \cdot [\nabla_0 \mathbf{r}(t)]^\top + \nabla_0 \mathbf{r}(t) \cdot \mathbf{L}^\top(t) \cdot [\nabla_0 \mathbf{r}(t)]^\top.$$

Introducing the rate-of-strain tensor

$$\mathbf{D}(t) = \frac{1}{2} [\mathbf{L}(t) + \mathbf{L}^\top(t)],$$

we obtain

$$\frac{d\mathbf{C}}{dt}(t) = 2 \nabla_0 \mathbf{r}(t) \cdot \mathbf{D}(t) \cdot [\nabla_0 \mathbf{r}(t)]^\top. \quad (24)$$

Equations (16), (20), (22) and (24) result in

$$\begin{aligned} \frac{d\mathbf{C}_e}{dt}(t) &= -\mathbf{L}_u(t) \cdot \mathbf{C}_e(t) - \mathbf{C}_e(t) \cdot \mathbf{L}_u^\top(t) \\ &\quad + 2 [\nabla_0 \mathbf{r}_u(t)]^{-1} \cdot \nabla_0 \mathbf{r}(t) \cdot \mathbf{D}(t) \cdot [\nabla_0 \mathbf{r}(t)]^\top \cdot [\nabla_0 \mathbf{r}_u(t)]^{-\top}. \end{aligned} \quad (25)$$

Bearing in mind that

$$\frac{d\mathbf{C}_e^{-1}}{dt}(t) = -\mathbf{C}_e^{-1}(t) \cdot \frac{d\mathbf{C}_e}{dt}(t) \cdot \mathbf{C}_e^{-1}(t),$$

we find from Eqs. (16) and (25) that

$$\begin{aligned} \frac{d\mathbf{C}_e^{-1}}{dt}(t) &= \mathbf{C}_e^{-1}(t) \cdot \mathbf{L}_u(t) + \mathbf{L}_u^\top(t) \cdot \mathbf{C}_e^{-1}(t) \\ &\quad - 2 [\nabla_0 \mathbf{r}_u(t)]^\top \cdot \mathbf{C}_e^{-1}(t) \cdot \nabla_0 \mathbf{r}(t) \cdot \mathbf{D}(t) \cdot [\nabla_0 \mathbf{r}(t)]^\top \cdot \mathbf{C}_e^{-1}(t) \cdot \nabla_0 \mathbf{r}_u(t). \end{aligned} \quad (26)$$

The first principal invariant of the tensor  $\mathbf{C}_e(t)$  is given by

$$I_1(\mathbf{C}_e) = \mathbf{C}_e : \mathbf{I},$$

where the colon stands for convolution. Differentiating this equality with respect to time and using Eq. (25), we obtain

$$\begin{aligned} \frac{dI_1}{dt}(\mathbf{C}_e(t)) &= -\mathbf{L}_u(t) : \mathbf{C}_e(t) - \mathbf{C}_e(t) : \mathbf{L}_u^\top(t) \\ &\quad + 2 [(\nabla_0 \mathbf{r}(t))^\top \cdot (\nabla_0 \mathbf{r}_u(t))^{-\top} \cdot (\nabla_0 \mathbf{r}_u(t))^{-1} \cdot \nabla_0 \mathbf{r}(t)] : \mathbf{D}(t). \end{aligned}$$

Combining this equality with Eq. (14) and introducing the rate-of-strain tensor for sliding of junctions

$$\mathbf{D}_u(t) = \frac{1}{2}[\mathbf{L}_u(t) + \mathbf{L}_u^\top(t)],$$

we arrive at the formula

$$\frac{dI_1}{dt}(\mathbf{C}_e(t)) = 2\left[(\nabla_0\mathbf{r}(t))^\top \cdot \mathbf{C}_u^{-1}(t) \cdot \nabla_0\mathbf{r}(t)\right] : \mathbf{D}(t) - 2\mathbf{C}_e(t) : \mathbf{D}_u(t). \quad (27)$$

It follows from Eqs. (19) and (27) that

$$\frac{dI_1}{dt}(\mathbf{C}_e(t)) = 2\left[\mathbf{B}_e(t) : \mathbf{D}(t) - \mathbf{C}_e(t) : \mathbf{D}_u(t)\right]. \quad (28)$$

The Cauchy deformation tensors for transitions from the reference state to the deformed state and from the reference state to the unloaded state are assumed to obey the incompressibility condition, which implies that

$$I_3(\mathbf{C}_e) = 1.$$

It follows from this equality that

$$I_2(\mathbf{C}_e(t)) = I_1(\mathbf{C}_e^{-1}(t)) = \mathbf{C}_e^{-1}(t) : \mathbf{I}. \quad (29)$$

We differentiate Eq. (29) with respect to time, use Eqs. (13), (14) and (26), and obtain

$$\begin{aligned} \frac{dI_2}{dt}(\mathbf{C}_e(t)) &= \mathbf{C}_e^{-1}(t) : \mathbf{L}_u(t) + \mathbf{L}_u^\top(t) : \mathbf{C}_e^{-1}(t) - 2\mathbf{D}(t) : \\ &\quad \left[ (\nabla_0\mathbf{r}(t))^\top \cdot \mathbf{C}^{-1}(t) \cdot \nabla_0\mathbf{r}_u(t) \cdot (\nabla_0\mathbf{r}_u(t))^\top \cdot \mathbf{C}^{-1}(t) \cdot \nabla_0\mathbf{r}(t) \right] \\ &= 2\mathbf{C}_e^{-1}(t) : \mathbf{D}_u(t) - 2\left[ (\nabla_0\mathbf{r}(t))^{-1} \cdot \mathbf{C}_u(t) \cdot (\nabla_0\mathbf{r}(t))^{-\top} \right] : \mathbf{D}(t). \end{aligned}$$

This equality together with Eq. (19) results in the formula

$$\frac{dI_2}{dt}(\mathbf{C}_e(t)) = -2\left[\mathbf{B}_e^{-1} : \mathbf{D}(t) - \mathbf{C}_e^{-1}(t) : \mathbf{D}_u(t)\right]. \quad (30)$$

Equations (28) and (30) determine the derivatives of the principal invariants of the tensor  $\mathbf{C}_e(t)$ .

Our goal now is to calculate the derivative of an arbitrary smooth function,  $\phi = \phi(I_1, I_2)$ , of the principal invariants,  $I_k$ , of the Cauchy deformation tensor,  $\mathbf{C}_e(t)$ , with respect to time. According to the chain rule for differentiation,

$$\frac{d\phi}{dt} = \phi_{,1}(I_1, I_2) \frac{dI_1}{dt} + \phi_{,2}(I_1, I_2) \frac{dI_2}{dt}, \quad (31)$$

where we use the notation

$$\phi_{,k} = \frac{\partial\phi}{\partial I_k}.$$

Substitution of expressions (28) and (30) into Eq. (31) implies that

$$\begin{aligned} \frac{d\phi}{dt}(I_1(\mathbf{C}_e(t)), I_2(\mathbf{C}_e(t))) &= 2[\phi_{,1}\mathbf{B}_e(t) - \phi_{,2}\mathbf{B}_e^{-1}(t)] : \mathbf{D}(t) \\ &\quad - 2[\phi_{,1}\mathbf{C}_e(t) - \phi_{,2}\mathbf{C}_e^{-1}(t)] : \mathbf{D}_u(t). \end{aligned} \quad (32)$$

Equation (32) generalizes the conventional formula for the derivative of a function  $\phi$  of the principal invariants,  $I_k$ , of the Cauchy deformation tensor  $\mathbf{C}(t)$ :

$$\frac{d\phi}{dt}(I_1(\mathbf{C}(t)), I_2(\mathbf{C}(t))) = 2[\phi_{,1}\mathbf{B}(t) - \phi_{,2}\mathbf{B}^{-1}(t)] : \mathbf{D}(t). \quad (33)$$

In what follows, we analyze deformation of meso-domains with various potential energies,  $\omega$ , where junctions start to slip with respect to the bulk material at various times,  $\tau$ , while before the instant  $\tau$ , they move together with the bulk medium. This means that the tensors  $\mathbf{B}_e$  and  $\mathbf{C}_e$  become functions of three variables,  $t$ ,  $\tau$  and  $\omega$ , which satisfy the initial conditions

$$\mathbf{B}_e(t, \tau, \omega)\Big|_{t=\tau} = \mathbf{B}(\tau), \quad \mathbf{C}_e(t, \tau, \omega)\Big|_{t=\tau} = \mathbf{C}(\tau). \quad (34)$$

It follows from Eq. (32) that the derivative of an arbitrary function  $\phi$  of the first two principal invariants of the Cauchy deformation tensor  $\mathbf{C}_e(t, \tau)$  reads

$$\begin{aligned} &\frac{\partial\phi}{\partial t}(I_1(\mathbf{C}_e(t, \tau, \omega)), I_2(\mathbf{C}_e(t, \tau, \omega))) \\ &= 2[\phi_{,1}\mathbf{B}_e(t, \tau, \omega) - \phi_{,2}\mathbf{B}_e^{-1}(t, \tau, \omega)] : \mathbf{D}(t) \\ &\quad - 2[\phi_{,1}\mathbf{C}_e(t, \tau, \omega) - \phi_{,2}\mathbf{C}_e^{-1}(t, \tau, \omega)] : \mathbf{D}_u(t, \tau, \omega). \end{aligned} \quad (35)$$

## 4 Strain energy of an elastomer

We confine ourselves to loading processes which causes an increase in the concentration of active meso-domains with time. This implies that any active meso-region can be entirely characterized by its potential energy,  $\omega$ , and the instant,  $\tau$ , when it becomes active. We set  $\tau = 0$  for regions active in the stress-free state.

The conventional affinity hypothesis is adopted for deformation of passive meso-domains. According to this assumption, thermal oscillations of junctions are disregarded and the deformation gradient for the motion of junctions at the micro-level is supposed to coincide with the deformation gradient for the movement of appropriate points of an elastomer at the macro-level (Treloar, 1975).

A passive region is treated as an isotropic incompressible medium, whose mechanical energy per strand,  $w$ , depends on the current temperature,  $T$  (the strong effect of temperature reflects the entropic nature of the strain energy for rubbery polymers), the measure of damage,  $\alpha$ , and the first two principal invariants,  $I_k$ , of the right Cauchy deformation tensor  $\mathbf{C}$ ,

$$w = w(\alpha(t), T(t), I_1(\mathbf{C}(t)), I_2(\mathbf{C}(t))). \quad (36)$$

At an arbitrary instant  $t \geq 0$ , the strain energy of a strand,  $w_0$ , belonging to a meso-domain with potential energy  $\omega$  which became active at instant  $\tau \in [0, t]$  is assumed to be a function of the current temperature,  $T$ , and the first two principal invariants of the right Cauchy deformation tensor  $\mathbf{C}_e$ ,

$$w_0 = w_0\left(T(t), I_1(\mathbf{C}_e(t, \tau, \omega)), I_2(\mathbf{C}_e(t, \tau, \omega))\right). \quad (37)$$

Equations (36) and (37) are based on the conventional hypothesis that the excluded-volume effect and other multi-chain effects are screened for an individual chain by surrounding macromolecules and are taken into account in terms of the incompressibility condition only (Everaers, 1998).

To simplify the analysis, the strain energy of a strand is assumed to be independent of the potential energy,  $\omega$ , of a meso-region to which this strand belongs (the latter means that the functions  $w$  and  $w_0$  are treated as average mechanical energies of strands). The mechanical energy of a strand in an active meso-region,  $w_0$ , differs, however, from the strain energy,  $w$ , of a strand in a passive domain. The functions  $w$  and  $w_0$  obey the conditions

$$w(\alpha, T, I_1, I_2)\Big|_{I_1=3, I_2=3} = 0, \quad w_0(T, I_1, I_2)\Big|_{I_1=3, I_2=3} = 0, \quad (38)$$

which express the fact that these strain energies vanish in the reference state. To establish a connection between the functions  $w$  and  $w_0$ , we suppose that for a passive meso-domain with a potential energy  $\omega$  and a damage measure  $\alpha$ , the mechanical energy reads

$$w(\alpha, T, I_1, I_2) = w_0(T, I_1, I_2) + \alpha \Delta w(T, I_1, I_2), \quad (39)$$

where  $\Delta w$  is the increment of mechanical energy per strand in a passive meso-domain caused by inter-chain interactions (van der Waals forces). Equation (39) implies that the strain energy density of an elastomer is continuous at the point of transition of a passive meso-domain into the active state (when the damage parameter,  $\alpha$ , vanishes).

Summing the mechanical energies for strands belonging to initial active meso-regions with various potential energies,  $\omega$ , to passive meso-domains with various energies,  $\omega$ , and damage measures,  $\alpha$ , as well as to meso-domains that become active at various instants,  $\tau \in [0, t]$ , we find the strain energy density per unit mass of an elastomer

$$\begin{aligned} W(t) = & \int_0^\infty d\omega \left[ \int_0^\infty \Xi_p(t, \alpha, \omega) w(\alpha, T(t), I_1(\mathbf{C}(t)), I_2(\mathbf{C}(t))) d\alpha \right. \\ & + X_a(0, \omega) w_0\left(T(t), I_1(\mathbf{C}_e(t, 0, \omega)), I_2(\mathbf{C}_e(t, 0, \omega))\right) \\ & \left. + \int_0^t \gamma(\tau, \omega) w_0\left(T(t), I_1(\mathbf{C}_e(t, \tau, \omega)), I_2(\mathbf{C}_e(t, \tau, \omega))\right) d\tau \right]. \end{aligned}$$

Substitution of Eqs. (36), (37) and (39) into this equality results in

$$\begin{aligned} W(t) = & N_p(t) w_0\left(T(t), I_1(\mathbf{C}(t)), I_2(\mathbf{C}(t))\right) + Z(t) \Delta w\left(T(t), I_1(\mathbf{C}(t)), I_2(\mathbf{C}(t))\right) \\ & + \int_0^\infty d\omega \left[ X_a(0, \omega) w_0\left(T(t), I_1(\mathbf{C}_e(t, 0, \omega)), I_2(\mathbf{C}_e(t, 0, \omega))\right) \right. \\ & \left. + \int_0^t \gamma(\tau, \omega) w_0\left(T(t), I_1(\mathbf{C}_e(t, \tau, \omega)), I_2(\mathbf{C}_e(t, \tau, \omega))\right) d\tau \right], \quad (40) \end{aligned}$$

where

$$Z(t) = \int_0^\infty \alpha d\alpha \int_0^\infty \Xi_p(t, \alpha, \omega) d\omega. \quad (41)$$

Our purpose now is to calculate the derivative of the function  $W(t)$  with respect to time. It follows from Eqs. (33), (35) and (40) that

$$\frac{dW}{dt}(t) = J(t) \frac{dT}{dt}(t) + 2\mathbf{\Lambda}(t) : \mathbf{D}(t) - Y_1(t) - Y_2(t), \quad (42)$$

where

$$\begin{aligned} J(t) &= N_p(t) \frac{\partial w_0}{\partial T}(T(t), I_1(\mathbf{C}(t)), I_2(\mathbf{C}(t))) + Z(t) \frac{\partial \Delta w}{\partial T}(T(t), I_1(\mathbf{C}(t)), I_2(\mathbf{C}(t))) \\ &\quad + \int_0^\infty d\omega \left[ X_a(0, \omega) \frac{\partial w_0}{\partial T}(T(t), I_1(\mathbf{C}_e(t, 0, \omega)), I_2(\mathbf{C}_e(t, 0, \omega))) \right. \\ &\quad \left. + \int_0^t \gamma(\tau, \omega) \frac{\partial w_0}{\partial T}(T(t), I_1(\mathbf{C}_e(t, \tau, \omega)), I_2(\mathbf{C}_e(t, \tau, \omega))) d\tau \right], \\ \mathbf{\Lambda}(t) &= N_p(t) \left( w_{0,1}(T(t), I_1(\mathbf{C}(t)), I_2(\mathbf{C}(t))) \mathbf{B}(t) \right. \\ &\quad \left. - w_{0,2}(T(t), I_1(\mathbf{C}(t)), I_2(\mathbf{C}(t))) \mathbf{B}^{-1}(t) \right) \\ &\quad + Z(t) \left( \Delta w_{,1}(T(t), I_1(\mathbf{C}(t)), I_2(\mathbf{C}(t))) \mathbf{B}(t) \right. \\ &\quad \left. - \Delta w_{,2}(T(t), I_1(\mathbf{C}(t)), I_2(\mathbf{C}(t))) \mathbf{B}^{-1}(t) \right) \\ &\quad + \int_0^\infty d\omega \left[ X_a(0, \omega) \left( w_{0,1}(T(t), I_1(\mathbf{C}_e(t, 0, \omega)), I_2(\mathbf{C}_e(t, 0, \omega))) \mathbf{B}_e(t, 0, \omega) \right. \right. \\ &\quad \left. \left. - w_{0,2}(T(t), I_1(\mathbf{C}_e(t, 0, \omega)), I_2(\mathbf{C}_e(t, 0, \omega))) \mathbf{B}_e^{-1}(t, 0, \omega) \right) \right. \\ &\quad \left. + \int_0^t \gamma(\tau, \omega) \left( w_{0,1}(T(t), I_1(\mathbf{C}_e(t, \tau, \omega)), I_2(\mathbf{C}_e(t, \tau, \omega))) \mathbf{B}_e(t, \tau, \omega) \right. \right. \\ &\quad \left. \left. - w_{0,2}(T(t), I_1(\mathbf{C}_e(t, \tau, \omega)), I_2(\mathbf{C}_e(t, \tau, \omega))) \mathbf{B}_e^{-1}(t, \tau, \omega) \right) d\tau \right], \\ Y_1(t) &= -\frac{dN_p}{dt}(t) w_0(T(t), I_1(\mathbf{C}(t)), I_2(\mathbf{C}(t))) \\ &\quad - \frac{dZ}{dt}(t) \Delta w(T(t), I_1(\mathbf{C}(t)), I_2(\mathbf{C}(t))) \\ &\quad - \int_0^\infty \gamma(t, \omega) w_0(T(t), I_1(\mathbf{C}_e(t, t, \omega)), I_2(\mathbf{C}_e(t, t, \omega))) d\omega, \\ Y_2(t) &= 2 \int_0^\infty \left[ X_a(0, \omega) \mathbf{\Lambda}_u(t, 0, \omega) : \mathbf{D}_u(t, 0, \omega) \right. \\ &\quad \left. + \int_0^t \gamma(\tau, \omega) \mathbf{\Lambda}_u(t, \tau, \omega) : \mathbf{D}_u(t, \tau, \omega) d\tau \right] d\omega, \\ \mathbf{\Lambda}_u(t, \tau, \omega) &= w_{0,1}(T(t), I_1(\mathbf{C}_e(t, \tau, \omega)), I_2(\mathbf{C}_e(t, \tau, \omega))) \mathbf{C}_e(t, \tau, \omega) \\ &\quad - w_{0,2}(T(t), I_1(\mathbf{C}_e(t, \tau, \omega)), I_2(\mathbf{C}_e(t, \tau, \omega))) \mathbf{C}_e^{-1}(t, \tau, \omega). \end{aligned} \quad (43)$$

Equations (7), (9), (34) and (43) imply that

$$Y_1(t) = -\frac{dZ}{dt}(t) \Delta w(T(t), I_1(\mathbf{C}(t)), I_2(\mathbf{C}(t))), \quad (44)$$

which means that the function  $Y_1$  is non-negative for an arbitrary program of loading with an increasing number of active meso-domains.

## 5 Constitutive equations

We confine ourselves to quasi-static loadings with finite strains, when mechanically induced changes in temperature,  $\Delta T$ , are rather weak. This implies that the effect of temperature on the specific heat,  $c$ , may be neglected. The following expression is adopted for the free energy (per unit mass) of a filled elastomer:

$$\Psi = \Psi_0 + (c - S_0)(T - T_0) - cT \ln \frac{T}{T_0} + W, \quad (45)$$

where  $\Psi_0$  and  $S_0$  are the free energy and the entropy per unit mass in the stress-free state at the reference temperature  $T_0$ . The second and third terms on the right-hand side of Eq. (45) characterize the free energy of thermal motion of chains.

For an incompressible medium, the Clausius–Duhem inequality reads (Haupt, 2000)

$$Q = -S \frac{dT}{dt} - \frac{d\Psi}{dt} + \frac{1}{\rho} (\boldsymbol{\Sigma}' : \mathbf{D} - \frac{1}{T} \mathbf{q} \cdot \nabla T) \geq 0, \quad (46)$$

where  $\rho$  is mass density,  $\boldsymbol{\Sigma}'$  is the deviatoric component of the Cauchy stress tensor  $\boldsymbol{\Sigma}$ ,  $\mathbf{q}$  is the heat flux vector,  $S$  is the entropy, and  $Q$  is the internal dissipation per unit mass. Substitution of Eqs. (42) and (45) into Eq. (46) results in

$$\begin{aligned} Q = & -\left(S - S_0 - c \ln \frac{T}{T_0} + J\right) \frac{dT}{dt} + \frac{1}{\rho} (\boldsymbol{\Sigma}' - 2\rho\boldsymbol{\Lambda}) : \mathbf{D} \\ & + Y_1 + Y_2 - \frac{1}{\rho T} \mathbf{q} \cdot \nabla T \geq 0. \end{aligned} \quad (47)$$

The term  $Y_1$  describes the energy dissipation driven by transition of passive meso-domains into the active state, the term  $Y_2$  characterizes the entropy production induced by slippage of junctions with respect to the bulk material, whereas the last term in Eq. (47) is responsible for internal dissipation caused by thermal conductivity.

Because Eq. (47) is to be satisfied for an arbitrary loading, the expressions in brackets vanish. This implies the formula for the entropy per unit mass

$$S(t) = S_0 + c \ln \frac{T(t)}{T_0} - J(t)$$

and the constitutive equation

$$\boldsymbol{\Sigma}(t) = -P(t)\mathbf{I} + 2\rho\boldsymbol{\Lambda}(t),$$

where  $P$  is pressure. Substitution of expression (43) into this equality implies the stress–strain relation

$$\boldsymbol{\Sigma}(t) = -P(t)\mathbf{I} + 2\rho \left\{ N_p(t) \left( w_{0,1}(T(t), I_1(\mathbf{C}(t)), I_2(\mathbf{C}(t))) \right) \mathbf{B}(t) \right.$$

$$\begin{aligned}
& -w_{0,2}\left(T(t), I_1(\mathbf{C}(t)), I_2(\mathbf{C}(t))\right)\mathbf{B}^{-1}(t) \\
& +Z(t)\left(\Delta w_{,1}\left(T(t), I_1(\mathbf{C}(t)), I_2(\mathbf{C}(t))\right)\mathbf{B}(t)\right. \\
& \left.-\Delta w_{,2}\left(T(t), I_1(\mathbf{C}(t)), I_2(\mathbf{C}(t))\right)\mathbf{B}^{-1}(t)\right) \\
& +\int_0^\infty\left[X_a(0, \omega)\left(w_{0,1}\left(T(t), I_1(\mathbf{C}_e(t, 0, \omega)), I_2(\mathbf{C}_e(t, 0, \omega))\right)\mathbf{B}_e(t, 0, \omega)\right.\right. \\
& \left.-w_{0,2}\left(T(t), I_1(\mathbf{C}_e(t, 0, \omega)), I_2(\mathbf{C}_e(t, 0, \omega))\right)\mathbf{B}_e^{-1}(t, 0, \omega)\right) \\
& \left.+\int_0^t\gamma(\tau, \omega)\left(w_{0,1}\left(T(t), I_1(\mathbf{C}_e(t, \tau, \omega)), I_2(\mathbf{C}_e(t, \tau, \omega))\right)\mathbf{B}_e(t, \tau, \omega)\right.\right. \\
& \left.\left.-w_{0,2}\left(T(t), I_1(\mathbf{C}_e(t, \tau, \omega)), I_2(\mathbf{C}_e(t, \tau, \omega))\right)\mathbf{B}_e^{-1}(t, \tau, \omega)\right)d\tau\right]d\omega\}. \quad (48)
\end{aligned}$$

We adopt the Fourier law for the heat flux vector  $\mathbf{q}$ ,

$$\mathbf{q} = -\kappa\nabla T,$$

where  $\kappa > 0$  is thermal diffusivity. It follows from this equation that the last term on the right-hand side of Eq. (47) is non-negative.

The incompressibility condition implies that the first invariant of the rate-of-strain tensor  $\mathbf{D}_u(t)$  vanishes, which means that

$$\mathbf{\Lambda}_u : \mathbf{D}_u = \mathbf{\Lambda}'_u : \mathbf{D}_u,$$

where the prime stands for the deviatoric component of a tensor. By analogy with Eq. (1), we postulate that the rate-of-strain tensor for sliding of junctions,  $\mathbf{D}_u$ , is proportional to the tensor  $\mathbf{\Lambda}'_u$ ,

$$\rho\mathbf{\Lambda}'_u(t, \tau, \omega) = \eta\mathbf{D}_u(t, \tau, \omega), \quad (49)$$

where  $\eta > 0$  is a viscosity. Equation (49) provides the flow rule for slippage of junctions with respect to the bulk material, which ensures that the term  $\mathbf{\Lambda}_u : \mathbf{D}_u$  is non-negative. It follows from this result and Eq. (43) that  $Y_2 \geq 0$  for an arbitrary program of straining. Because the function  $Y_1$  is non-negative as well, governing equations (48) and (49) guarantee that the dissipation inequality (47) is fulfilled.

It follows from Eqs. (2), (4), (43) and (49) that

$$\begin{aligned}
\mathbf{D}_u(t, \tau, \omega) & = \frac{\rho\Gamma_0}{G}\exp(-\omega)\left[w_{0,1}\left(T(t), I_1(\mathbf{C}_e(t, \tau, \omega)), I_2(\mathbf{C}_e(t, \tau, \omega))\right)\mathbf{C}'_e(t, \tau, \omega)\right. \\
& \left.-w_{0,2}\left(T(t), I_1(\mathbf{C}_e(t, \tau, \omega)), I_2(\mathbf{C}_e(t, \tau, \omega))\right)\left(\mathbf{C}_e^{-1}(t, \tau, \omega)\right)'\right]. \quad (50)
\end{aligned}$$

Formulas (48) and (50) entirely determine the evolution of an ensemble of meso-regions in an elastomer. These equations may be noticeably simplified provided that the conventional theory of rubber elasticity is applied to the description of the mechanical energy in active meso-domains (Treloar, 1975). Setting

$$\rho w_0 = G(I_1 - 3), \quad (51)$$

which corresponds to the strain energy density of a neo-Hookean material, we find that

$$\begin{aligned}
\Sigma(t) = & -P(t)\mathbf{I} + 2G\left\{N_p(t)\mathbf{B}(t) + \int_0^\infty \left[X_a(0, \omega)\mathbf{B}_e(t, 0, \omega) \right. \right. \\
& \left. \left. + \int_0^t \gamma(\tau, \omega)\mathbf{B}_e(t, \tau, \omega)d\tau\right]d\omega\right\} \\
& + 2\rho Z(t)\left[\Delta w_{,1}(T(t), I_1(\mathbf{C}(t)), I_2(\mathbf{C}(t)))\mathbf{B}(t) \right. \\
& \left. - \Delta w_{,2}(T(t), I_1(\mathbf{C}(t)), I_2(\mathbf{C}(t)))\mathbf{B}^{-1}(t)\right]
\end{aligned} \tag{52}$$

and

$$\mathbf{D}_u(t, \tau, \omega) = \Gamma_0 \exp(-\omega)\mathbf{C}'_e(t, \tau, \omega). \tag{53}$$

## 6 Uniaxial tension of a specimen

Constitutive equations (52) and (53) are now applied to analyze stresses in a bar under tension. Points of the bar refer to Cartesian coordinates  $\{X_i\}$  in the stress-free state and to Cartesian coordinates  $\{x_i\}$  in the deformed state, ( $i = 1, 2, 3$ ). Uniaxial tension of an incompressible medium is described by the formulas

$$x_1 = k(t)X_1, \quad x_2 = k^{-\frac{1}{2}}(t)X_2, \quad x_3 = k^{-\frac{1}{2}}(t)X_3, \tag{54}$$

where  $k = k(t)$  is the extension ratio. We assume that transition from the reference state to the unloaded state is determined by equations similar to Eq. (54),

$$\xi_1 = k_u(t, \tau, \omega)X_1, \quad \xi_2 = k_u^{-\frac{1}{2}}(t, \tau, \omega)X_2, \quad \xi_3 = k_u^{-\frac{1}{2}}(t, \tau, \omega)X_3, \tag{55}$$

where  $\{\xi_i\}$  are Cartesian coordinates in the unloaded configuration and  $k_u(t, \tau, \omega)$  is a function to be found. The Cauchy deformation tensors,  $\mathbf{B}(t)$  and  $\mathbf{C}(t)$ , are given by

$$\mathbf{B}(t) = \mathbf{C}(t) = k^2(t)\mathbf{e}_1\mathbf{e}_1 + k^{-1}(t)(\mathbf{e}_2\mathbf{e}_2 + \mathbf{e}_3\mathbf{e}_3), \tag{56}$$

where  $\mathbf{e}_i$  are base vectors of the frame  $\{X_i\}$ . The Cauchy deformation tensors,  $\mathbf{B}_e(t, \tau, \omega)$  and  $\mathbf{C}_e(t, \tau, \omega)$ , are determined by the formula

$$\mathbf{B}_e(t, \tau, \omega) = \mathbf{C}_e(t, \tau, \omega) = \left(\frac{k(t)}{k_u(t, \tau, \omega)}\right)^2 \mathbf{e}_1\mathbf{e}_1 + \frac{k_u(t, \tau, \omega)}{k(t)}(\mathbf{e}_2\mathbf{e}_2 + \mathbf{e}_3\mathbf{e}_3), \tag{57}$$

which implies that

$$\mathbf{C}'_e(t, \tau, \omega) = \frac{2}{3}\left[\left(\frac{k(t)}{k_u(t, \tau, \omega)}\right)^2 - \frac{k_u(t, \tau, \omega)}{k(t)}\right]\left[\mathbf{e}_1\mathbf{e}_1 - \frac{1}{2}(\mathbf{e}_2\mathbf{e}_2 + \mathbf{e}_3\mathbf{e}_3)\right]. \tag{58}$$

It follows from Eq. (55) that

$$\mathbf{D}_u(t, \tau, \omega) = \frac{1}{k_u(t, \tau, \omega)} \frac{\partial k_u}{\partial t}(t, \tau, \omega) \left[\mathbf{e}_1\mathbf{e}_1 - \frac{1}{2}(\mathbf{e}_2\mathbf{e}_2 + \mathbf{e}_3\mathbf{e}_3)\right]. \tag{59}$$

Substitution of expressions (58) and (59) into the flow rule (53) implies that the function  $k_u(t, \tau, \omega)$  satisfies the differential equation

$$\frac{1}{k_u(t, \tau, \omega)} \frac{\partial k_u}{\partial t}(t, \tau, \omega) = \Gamma_* \exp(-\omega) \left[ \left( \frac{k(t)}{k_u(t, \tau, \omega)} \right)^2 - \frac{k_u(t, \tau, \omega)}{k(t)} \right] \quad (60)$$

with the initial condition

$$k_u(t, \tau, \omega) \Big|_{t=\tau} = 1. \quad (61)$$

The coefficient  $\Gamma_*$  in Eq. (60) reads

$$\Gamma_* = \frac{2}{3} \Gamma_0.$$

The non-zero components  $\Sigma_k$  of the Cauchy stress tensor

$$\Sigma = \Sigma_1 \mathbf{e}_1 \mathbf{e}_1 + \Sigma_2 (\mathbf{e}_2 \mathbf{e}_2 + \mathbf{e}_3 \mathbf{e}_3)$$

are given by

$$\begin{aligned} \Sigma_1(t) &= -P(t) + 2\rho Z(t) [\Delta w_{,1} k^2(t) - \Delta w_{,2} k^{-2}(t)] + 2Gk^2(t) \left\{ N_p(t) \right. \\ &\quad \left. + \int_0^\infty [X_a(0, \omega) k_u^{-2}(t, 0, \omega) + \int_0^t \gamma(\tau, \omega) k_u^{-2}(t, \tau, \omega) d\tau] d\omega \right\}, \\ \Sigma_2(t) &= -P(t) + 2\rho Z(t) [\Delta w_{,1} k^{-1}(t) - \Delta w_{,2} k(t)] + 2Gk^{-1}(t) \left\{ N_p(t) \right. \\ &\quad \left. + \int_0^\infty [X_a(0, \omega) k_u(t, 0, \omega) + \int_0^t \gamma(\tau, \omega) k_u(t, \tau, \omega) d\tau] d\omega \right\}, \end{aligned}$$

where arguments of the function  $\Delta w$  are omitted for simplicity. Excluding the unknown pressure  $P(t)$  from the expressions for  $\Sigma_k$  with the help of the boundary condition

$$\Sigma_2(t) = 0,$$

we find the longitudinal stress

$$\begin{aligned} \Sigma_1(t) &= 2 \left[ GN_p(t) + \rho Z(t) (\Delta w_{,1} + k^{-1}(t) \Delta w_{,2}) \right] (k^2(t) - k^{-1}(t)) \\ &\quad + 2G \int_0^\infty \left[ X_a(0, \omega) \left( \left( \frac{k(t)}{k_u(t, 0, \omega)} \right)^2 - \frac{k_u(t, 0, \omega)}{k(t)} \right) \right. \\ &\quad \left. + \int_0^t \gamma(\tau, \omega) \left( \left( \frac{k(t)}{k_u(t, \tau, \omega)} \right)^2 - \frac{k_u(t, \tau, \omega)}{k(t)} \right) d\tau \right] d\omega. \end{aligned} \quad (62)$$

Equations (60) to (62) determine the stress in a specimen for an arbitrary program of straining. To compare results of numerical simulation with experimental data, we focus on a tensile relaxation test with

$$k(t) = \begin{cases} 1, & t < 0, \\ \lambda, & t > 0, \end{cases} \quad (63)$$

where  $\lambda > 1$  is a constant.

For the loading program (63),  $\Delta w_{,1}$  and  $\Delta w_{,2}$  become functions of  $\lambda$  only,

$$\Delta w_{,k} = \Delta w_{,k}(\lambda) \quad (k = 1, 2).$$

We suppose that the concentration of active meso-regions changes at the instant  $t = 0$  only, which means that the function  $\gamma(t, \omega)$  vanishes for  $t > 0$ . The quantities  $N_p$  and  $Z$  are determined by the elongation ratio,  $\lambda$ , only,

$$N_p = N_p(\lambda), \quad Z = Z(\lambda).$$

The number of active meso-domains per unit mass,  $X_a(0, \omega)$ , becomes a function of  $\lambda$ ,

$$X_a(0, \omega) = N_a(\lambda)p(\lambda, \omega),$$

where  $N_a(\lambda)$  is the number of active regions at stretching to the elongation ratio  $\lambda$ , and  $p(\lambda, \omega)$  is the distribution function for meso-domains with various potential energies, which satisfies the condition

$$\int_0^\infty p(\lambda, \omega) d\omega = 1. \quad (64)$$

Finally, the quantity  $k_u(t, 0, \omega)$  also becomes a function of  $\lambda$ ,

$$k_u(t, 0, \omega) = h(t, \lambda, \omega).$$

Using Eqs. (10), (11) and introducing the notation,

$$\begin{aligned} \psi_1(\lambda) &= 2 \left[ GN + \rho Z(\lambda) (\Delta w_{,1}(\lambda) + \lambda^{-1} \Delta w_{,2}(\lambda)) \right] (\lambda^2 - \lambda^{-1}), \\ \psi_2(\lambda) &= 2GN_a(\lambda) (\lambda^2 - \lambda^{-1}), \end{aligned} \quad (65)$$

we find from Eqs. (62) and (63) that

$$\Sigma_1(t, \lambda) = \psi_1(\lambda) - \psi_2(\lambda) \int_0^\infty [1 - f(t, \lambda, \omega)] p(\lambda, \omega) d\omega, \quad (66)$$

where

$$f(t, \lambda, \omega) = (\lambda^2 - \lambda^{-1})^{-1} \left[ \left( \frac{\lambda}{h(t, \lambda, \omega)} \right)^2 - \frac{h(t, \lambda, \omega)}{\lambda} \right]. \quad (67)$$

It follows from Eqs. (60), (61) and (63) that the function  $h(t, \lambda, \omega)$  obeys the differential equation

$$\frac{\partial h}{\partial t}(t, \lambda, \omega) = \Gamma_* \exp(-\omega) \left[ \left( \frac{\lambda}{h(t, \lambda, \omega)} \right)^2 - \frac{h(t, \lambda, \omega)}{\lambda} \right] h(t, \lambda, \omega), \quad h(0, \lambda, \omega) = 1. \quad (68)$$

Equations (64) and (66) imply that the dimensionless ratio

$$R(t, \lambda) = \frac{\Sigma_1(t, \lambda)}{\Sigma_1(0, \lambda)}$$

is given by

$$R(t, \lambda) = 1 - A(\lambda) \int_0^\infty [1 - f(t, \lambda, \omega)] p(\lambda, \omega) d\omega, \quad (69)$$

where

$$A(\lambda) = \frac{\psi_2(\lambda)}{\psi_1(\lambda)}. \quad (70)$$

To fit experimental data, we employ the quasi-Gaussian distribution function

$$p(\lambda, \omega) = p_0(\lambda) \exp\left[-\frac{(\omega - \langle\omega(\lambda)\rangle_0)^2}{2\sigma^2(\lambda)}\right], \quad (71)$$

where  $\langle\omega\rangle_0$  and  $\sigma$  are adjustable parameters and  $p_0$  is determined by condition (64). Substitution of expression (71) into Eq. (69) results in

$$R(t, \lambda) = 1 - A(\lambda)p_0(\lambda) \int_0^\infty [1 - f(t, \lambda, \omega)] \left[-\frac{(\omega - \langle\omega(\lambda)\rangle_0)^2}{2\sigma^2(\lambda)}\right] d\omega.$$

Introducing the new variable,  $z = \omega - \omega_*$ , where  $\omega_* = \ln \Gamma_*$ , we obtain

$$R(t, \lambda) = 1 - A(\lambda)p_0(\lambda) \int_{-\omega_*}^\infty [1 - f(t, \lambda, z)] \left[-\frac{(z - \langle\omega(\lambda)\rangle)^2}{2\sigma^2(\lambda)}\right] dz,$$

where  $\langle\omega\rangle = \langle\omega\rangle_0 - \omega_*$ . Assuming the relative width of the quasi-Gaussian distribution,

$$\zeta = \frac{\sigma}{\langle\omega\rangle} \quad (72)$$

to be small compared to  $\langle\omega\rangle$  (this hypothesis will be discussed later), we neglect the integral over the interval  $[-\omega_*, 0]$  and find that

$$R(t, \lambda) = 1 - A(\lambda)p_0(\lambda) \int_0^\infty [1 - f(t, \lambda, z)] \left[-\frac{(z - \langle\omega(\lambda)\rangle)^2}{2\sigma^2(\lambda)}\right] dz, \quad (73)$$

where the function  $f(t, \lambda, z)$  is determined by Eq. (67). According to Eq. (68), the function  $h(t, \lambda, z)$  satisfies the differential equation

$$\frac{\partial h}{\partial t}(t, \lambda, z) = \exp(-z) \left[ \left( \frac{\lambda}{h(t, \lambda, z)} \right)^2 - \frac{h(t, \lambda, z)}{\lambda} \right] h(t, \lambda, z), \quad h(0, \lambda, z) = 1. \quad (74)$$

Equations (73) and (74) are determined by 3 dimensionless parameters:

1. the ratio,  $A$ , of the relaxing stress to the total stress at the beginning of the relaxation test;
2. the average potential energy,  $\langle\omega\rangle$ , for sliding of junctions in active in meso-domains;
3. the standard deviation of the potential energy,  $\sigma$ .

## 7 Experimental procedure

Three series of uniaxial relaxation tests were performed at room temperature. Dumb-bell specimens were provided by TARRC laboratories (Hertford, UK) and were used as received. The tests were executed on compound EDS-16 on the base of natural rubber reinforced by high abrasion furnace black. The compound contains 45 phr of carbon black. The mean diameter of filler particles is estimated as 30 nm, and their surface area is about 80 m<sup>2</sup>/g (Jäger and McQueen, 2001). A detailed formulation of the compound is presented in Table 1.

Experiments were carried out by using a testing machine designed at the Institute of Physics (Vienna, Austria) and equipped with a video-controlled system. To measure the longitudinal strain, two reflection lines were drawn in the central part of each specimen before loading (with the distance 7 mm between them). Changes in the distance between these lines were measured by a video-extensometer (with the accuracy of about 1 %). The tensile force was measured by using a standard loading cell. The nominal stress was determined as the ratio of the axial force to the cross-sectional area of a specimen in the stress-free state, 4 mm × 1 mm.

To analyze the effects of mechanical pre-loading and thermal recovery, the following testing procedure was chosen:

1. Any specimen was loaded with the strain rate  $\dot{\epsilon}_+ = 3.0 \cdot 10^{-2} \text{ s}^{-1}$  up to a given elongation ratio  $\lambda$ , which was preserved constant during the relaxation test ( $t_r = 1$  hour), and unloaded with the strain rate  $\dot{\epsilon}_- = -\dot{\epsilon}_+$ .
2. The specimen was annealed for  $t_a = 24$  hours at room temperature.
3. The specimen was loaded with the strain rate  $\dot{\epsilon}_+$  up to the elongation ratio  $\lambda_{\max} = 4.0$  and unloaded with the strain rate  $\dot{\epsilon}_-$ .
4. The specimen was annealed for  $t_a$  at ambient temperature.
5. The specimen was loaded with the strain rate  $\dot{\epsilon}_+$  up to the same elongation ratio,  $\lambda$ , as in the first test. This elongation ratio was preserved constant during the relaxation test, and, afterwards, the specimen was unloaded with the strain rate  $\dot{\epsilon}_-$ .
6. The specimen was recovered in an oven for 24 hours at the constant temperature  $T = 100 \text{ }^\circ\text{C}$  and cooled down by air to room temperature for 4 hours.
7. The specimen was loaded with the strain rate  $\dot{\epsilon}_+$  up to the same elongation ratio as in the first test. This elongation ratio was preserved constant during the relaxation test, and, afterwards, the specimen was unloaded with the strain rate  $\dot{\epsilon}_-$ .

The relaxation tests were carried out at four elongation ratios:  $\lambda_1 = 2.0$ ,  $\lambda_2 = 2.5$ ,  $\lambda_3 = 3.0$ , and  $\lambda_4 = 3.5$ .

The longitudinal stress  $\sigma$  was measured as a function of time  $t$  (the initial instant  $t = 0$  corresponds to the beginning of the relaxation test). For any elongation ratio,  $\lambda$ , the dimensionless ratio  $R(t, \lambda)$  is depicted versus the logarithm of time ( $\log = \log_{10}$ ) in Figures 1 to 3.

These figures evidence that the longitudinal stress is noticeably decreased during the relaxation time,  $t_r = 1$  h. For virgin specimens, this decrease equals 19.7 % at the elongation ratio  $\lambda_1$  and it reaches 27.9 % at  $\lambda_4$ .

After pre-loading to  $\lambda_{\max}$  and subsequent unloading, the time-dependent decrease in the stress is weakened. The portion of the longitudinal stress relaxed during  $t_r$  is estimated as 14.4 % at the elongation ratio  $\lambda_1$  and as 20.0 % at  $\lambda_4$ .

Thermal recovery of specimens at the elevated temperature  $T$  for  $t_a = 24$  h returns the specimens to their initial state. The decrease in the longitudinal stress during  $t_r = 1$  h is estimated as 19.7 % at the smallest elongation ratio,  $\lambda_1$ , and it grows up to 27.0 % at straining with  $\lambda_4$ .

These changes in the time-dependent behavior of the CB filled natural rubber are associated at the micro-level with the alternation of the internal structure of the compound:

- the concentration of active domains per unit mass grows with an increase in the elongation ratio,
- it noticeably decreases under pre-loading and subsequent unloading,
- this number returns (practically) to its initial value after thermal recovery.

To verify these assertions, we determine adjustable parameters in Eqs. (73) and (74) by matching experimental data and study the effect of the longitudinal ratio,  $\lambda$ , on the coefficients  $A$ ,  $\langle\omega\rangle$  and  $\sigma$ .

## 8 Comparison with experimental data

Given an elongation ratio,  $\lambda$ , the fitting procedure consists in the following. We fix intervals  $[0, \langle\omega\rangle_{\max}]$  and  $[0, \sigma_{\max}]$  where the “best-fit” parameters  $\langle\omega\rangle$  and  $\sigma$  are assumed to be found and divide these intervals into  $J$  subintervals by points  $\langle\omega\rangle_j = j\Delta_\omega$  and  $\sigma_j = j\Delta_\sigma$  with  $j = 1, \dots, J$ ,  $\Delta_\omega = \langle\omega\rangle_{\max}/J$  and  $\Delta_\sigma = \sigma_{\max}/J$ . For any pair of parameters  $\langle\omega\rangle_i$  and  $\sigma_j$ , we find the constant  $p_0$  from condition (64), where the integral is evaluated numerically. Afterwards, we calculate the integral in Eq. (73) and determine the pre-factor  $A = A(i, j)$  [which ensures the best fit of the experimental curve  $R_{\text{exp}}(t, \lambda)$ ] by the least-squares method. As a measure of deviations between observations and results of numerical analysis, we chose the function

$$r(i, j) = \sum_{t_k} \left[ R_{\text{exp}}(t_k, \lambda) - R_{\text{num}}(t_k, \lambda) \right]^2, \quad (75)$$

where the sum is calculated over all experimental points depicted in Figures 1 to 3 and the function  $R_{\text{num}}(t, \lambda)$  is determined by Eq. (73). Finally, the “best-fit” parameters  $\langle\omega\rangle$  and  $\sigma$  are determined as those which minimize the functional (75) on the set

$$\left\{ \langle\omega\rangle_i, \sigma_j \quad (i, j = 1, \dots, J) \right\}.$$

To ensure a high level of accuracy in the approximation of experimental data, after determining the “optimal” parameters  $\langle\omega\rangle_i$  and  $\sigma_j$ , this procedure is repeated for the new

intervals  $[\langle\omega\rangle_{i-1}, \langle\omega\rangle_{i+1}]$  and  $[\sigma_{j-1}, \sigma_{j+1}]$ . In the numerical analysis, we set  $\langle\omega\rangle_{\max} = 10.0$ ,  $\sigma_{\max} = 10.0$  and  $J = 20$ . The integrals in Eqs. (64) and (73) are calculated by using Simpson's method with 100 points and the step  $\Delta z = 0.2$ . For any  $z$ , the ordinary differential equation (74) was solved by the Runge–Kutta method with the time step  $\Delta t = 0.2$  s.

To assess the effect of straining of the average energy for sliding,  $\langle\omega\rangle$ , and the standard deviation of energy,  $\sigma$ , we plot these quantities versus the first invariant,  $I_1$ , of the Cauchy deformation tensor  $\mathbf{C}$ . It follows from Eq. (56) that in tensile relaxation tests,

$$I_1 = \lambda^2 + 2\lambda^{-1}.$$

Experimental data are approximated by the linear functions

$$\langle\omega\rangle = \omega_0 + \omega_1(I_1 - 3), \quad \sigma = \sigma_0 + \sigma_1(I_1 - 3), \quad (76)$$

where the coefficients  $\omega_k$  and  $\sigma_k$  are determined by the least-squares technique. These parameters are listed in Table 2. Figures 4 and 5 evidence that phenomenological relations (76) ensure good accuracy of fitting.

To provide some physical basis for Eq. (76), we refer to formula (51) that implies that for a neo–Hookean medium, the difference  $I_1 - 3$  serves as a measure of the mechanical energy of active meso-regions. Equations (76) show that the parameters  $\langle\omega\rangle$  and  $\sigma$  of the distribution function for potential energies of active domains are proportional to their average mechanical energy.

It follows from Eqs. (67) and (68) that  $f(0, \lambda, \omega) = 1$  and  $f(\infty, \lambda, \omega) = 0$ , which, together with Eqs. (64) and (66), yield

$$\Sigma_1(0, \lambda) = \psi_1(\lambda), \quad \Sigma_1(\infty, \lambda) = \psi_1(\lambda) - \psi_2(\lambda). \quad (77)$$

We associate  $\Sigma_1(\infty, \lambda)$  with the equilibrium stress,  $\Sigma_{\text{eq}}(\lambda)$ , and  $\Delta\Sigma(\lambda) = \Sigma_1(0, \lambda) - \Sigma_1(\infty, \lambda)$  with the relaxing stress. It follows from Eqs. (70) and (77) that the ratio

$$a(\lambda) = \frac{\Delta\Sigma(\lambda)}{\Sigma_{\text{eq}}(\lambda)} \quad (78)$$

reads

$$a(\lambda) = \frac{A(\lambda)}{1 - A(\lambda)}.$$

Using the values of  $A(\lambda)$  determined by fitting observations, we calculate the dimensionless ratio  $a(\lambda)$  and plot it versus the first invariant,  $I_1$ , of the Cauchy deformation tensor. Figure 6 demonstrates that the experimental data are correctly approximated by the linear relation

$$a = a_0 + a_1(I_1 - 3), \quad (79)$$

where the coefficients  $a_k$  are found by the least-squares algorithm and are collected in Table 2.

Figure 4 demonstrates that the average energy for sliding of junctions increases with the elongation ratio  $\lambda$ . This finding may be explained by the fact that only meso-domains

with low potential energies are active in a stress-free state, whereas regions with higher potential energies become involved in the sliding process provided that sufficiently large tension is applied to the specimen. The rate of growth of the average potential energy for sliding,  $\langle\omega\rangle$ , with  $I_1$  is relatively small for virgin specimens and it noticeably grows after pre-loading. After thermal recovery, changes in the function  $\langle\omega\rangle(I_1)$  become similar to those for a virgin sample. The loading–unloading procedure with  $\lambda_{\max} = 4.0$  results in a decrease of the average potential energy of the ensemble of active meso-regions for a stress-free specimen (the parameter  $\omega_0$  is reduced by 12 %). This inference may be explained by (at least) two reasons:

1. damage of the rubbery compound during pre-loading “turns off” some active regions in a virgin sample which become passive under unloading;
2. stretching of a specimen to a high elongation ratio and subsequent unloading result in a decrease in the potential energy of active regions, which, according to Eq. (68), is tantamount to an increase in the mean rate of slippage of junctions with respect to the bulk medium.

Figure 5 shows that the standard deviation of potential energies,  $\sigma$ , increases with the elongation ratio,  $\lambda$ . This growth is rather modest for virgin and recovered samples, but it becomes stronger after pre-loading: the coefficient  $\sigma_1$  for the pre-loaded specimens exceeds that for the virgin specimens by a factor of 3.5. After stretching of specimens to  $\lambda_{\max}$  and subsequent unloading, the quasi-Gaussian distribution of potential energies becomes substantially sharper: the standard deviation of energies for a stress-free rubbery compound,  $\sigma_0$ , is decreased by twice compared to the virgin material. This may be explained by the fact that pre-loading induces transformation of active meso-domains with relatively high potential energies (which characterize a “tail” of the Gaussian function with large values of  $\omega$ ) into the passive state. Thermal recovery at an elevated temperature “activates” a part of these regions (the corresponding curve in Figure 5 is located higher than the curve for samples suffered pre-loading), but no total recovery is observed: the graph of the function  $\sigma(I_1)$  for the recovered compound does not reach that for the virgin medium.

To evaluate the dimensionless width of the quasi-Gaussian distribution function (71), we calculate the ratio  $\zeta$  with the help of Eq. (72) and plot it versus the first invariant,  $I_1$ , of the Cauchy deformation tensor  $\mathbf{C}$  in Figure 7. Experimental data are approximated by the linear dependence

$$\zeta = \zeta_0 + \zeta_1(I_1 - 3), \quad (80)$$

where the constants  $\zeta_0$  and  $\zeta_1$  are determined by the least-squares algorithm (see Table 2). Figure 7 demonstrates fair agreement between observations and predictions of the phenomenological equation (80).

According to Figure 7, the dimensionless ratio  $\zeta$  is located within the interval between 0.4 and 0.8 for all specimens, which implies that the width of the distribution function (71) is relatively small. The latter may be thought of as a confirmation of the assumptions employed in the derivation of Eq. (73). The quantity  $\zeta$  decreases with the elongation ratio  $\lambda$  for virgin and recovered specimens, and it remains practically constant for pre-loaded samples. The maximal width of the quasi-Gaussian distribution is observed for the virgin

material. The distribution of potential energies for sliding of junctions in active meso-regions,  $p(\omega)$ , becomes substantially sharper after pre-loading, whereas thermal recovery results in widening of this distribution.

The ratio of the relaxing stress to the equilibrium stress,  $a$ , is plotted in Figure 6 as a function of the extension ratio,  $\lambda$ . This figure demonstrates that  $a$  is strongly influenced by stretching. For example,  $a$  grows by twice for virgin specimens when  $\lambda$  increases from 2.0 to 3.5. Equations (65), (77) and (78) imply that

$$a(\lambda) = \frac{N_a(\lambda)}{N_p(\lambda) + \rho G^{-1} Z(\lambda) [\Delta w_{,1}(\lambda) + \lambda^{-1} \Delta w_{,2}(\lambda)]}. \quad (81)$$

Because the term in brackets in Eq. (81) is an increasing function of  $\lambda$ , the growth of  $a(\lambda)$  is associated with the following phenomena occurring simultaneously:

1. micro-damage of passive meso-regions which results in a decrease of the function  $Z(\lambda)$ ,
2. transformation of passive domains into the active state. The latter is equivalent to an increase in  $N_a(\lambda)$  and a corresponding decrease in  $N_p(\lambda)$  which is connected with  $N_a(\lambda)$  by the conservation law (10).

To assess the effect of these two sources for changes in  $a(\lambda)$ , a constitutive model is necessary for damage of passive meso-regions. This model will be the subject of a subsequent publication.

Straining of samples to  $\lambda_{\max}$  and subsequent unloading result in a pronounced decrease in  $a$ , which is partially recovered after annealing at an elevated temperature. This severe decrease (the ratio for the relaxing stress to the equilibrium stress in pre-loaded specimens at relatively small strains,  $a_0$ , equals about 60 % of its value for virgin samples) reflects slowing down of time-dependent changes in the ratio  $R(t, \lambda)$  observed by comparison of the relaxation curves depicted in Figures 1 and 2. We suppose that this decrease in  $a_0$  is closely connected with the Mullins effect observed in loading–unloading tests on particle-reinforced elastomers.

Let us consider a particular case of the model where the function  $\Xi_p$  is independent of time (or the current strain for a time-dependent program of loading). This implies that the parameters  $N_a$ ,  $N_p$  and  $Z$  remain constants, and  $\gamma$  vanishes. Under these assumptions, the stress–strain relations (52) and (53) are reduced to the constitutive equations for a rheological model consisting of a nonlinear spring (which is characterized by the strain energy  $\Delta w$ ) connected in parallel with an infinite array of Maxwell’s elements [neo–Hookean springs linked in series with nonlinear dashpots whose response is described by Eq. (53)]. The latter model with a finite number of Maxwell’s elements has been widely used in the analysis of the viscoelastic and viscoplastic behavior of filler rubbers in the past decade, see, e.g., Govindjee and Simo (1992), Kaliske and Rothert (1998), Haupt and Sedlan (2001), to mention a few. Fitting observations in relaxation tests evidences that the sphere of applicability of this rheological model is rather limited, because it does not capture noticeable changes in the parameters  $\langle \omega \rangle$ ,  $\sigma$  and  $a$  with the elongation ratio  $\lambda$ . Our approach may be treated as an extension of this conventional model, where the effect of mechanical factors is taken into account on the number of Maxwell’s elements and viscosities of dashpots.

## 9 Concluding remarks

Constitutive equations have been derived for the time-dependent behavior of particle-reinforced elastomers at finite strains. A filled rubber is considered as an ensemble of meso-domains where junctions between macromolecules (chemical and physical cross-links and entanglements) are not fixed in the bulk medium, but they can slip with respect to it. To develop stress–strain relations, a version of the mean-field approach is employed: a complicated micro-structure of an elastomer reinforced by aggregates of filler is modelled as an equivalent network of macromolecules belonging to regions with various potential energies,  $\omega$ , for sliding of junctions. The distribution of potential energies of these meso-domains reflects

1. impurities and local non-homogeneities in the spatial distribution of a cross-linker (which is typical of both unfilled and filled elastomers),
2. density fluctuations driven by segregation of short chains to the interfaces between filler particles and the host medium,
3. severe micro-stresses in the neighborhoods of filler clusters in a strained elastomer caused by the strong difference in the elastic moduli of filler and rubber.

It is assumed that junctions slip with respect to the bulk material in active meso-domains, and the rate of sliding is determined by the conventional Boltzmann formula. Sliding of junctions in passive meso-regions is prevented by surrounding macromolecules [by means of inter-chain links which are (partially) ruptured under loading]. The concentration of links that forbid sliding is described by a measure of micro-damage,  $\alpha$ . Transition of a passive meso-domain in its active state occurs when the number of van der Waals links preventing sliding of junctions vanishes.

The mechanical energy of a filled elastomer is determined as the sum of strain energies of chains in active and passive meso-domains and the energy of interaction between macromolecules in passive regions. Constitutive equations for a filled elastomer are derived by using the laws of thermodynamics (we confine ourselves to active loading, when the concentration of active meso-domains does not decrease with time). These equations are applied for the study of stresses in an incompressible bar under uniaxial tension.

To validate the model, three series of tensile relaxation tests have been performed on carbon black filled natural rubber at elongations up to 350 %. In the first series of tests, virgin specimens are used, in the second series, relaxation experiments were carried out on the samples after mechanical pre-loading, and in the third series of tests, the time-dependent response was analyzed for the same specimens after recovery at an elevated temperature. Figures 1 to 3 demonstrate fair agreement between results of numerical simulation and observations.

To describe quantitatively changes in the internal structure of a particle-reinforced elastomer induced by pre-loading and thermal recovery, we presume that the distribution of potential energies for sliding of junctions may be approximated by a quasi-Gaussian function with two adjustable parameters. It is revealed that the average potential energy and the standard deviation of energies for sliding grow with the elongation ratio,  $\lambda$ . After the loading–unloading procedure, these parameters are noticeably reduced, which

is associated with “turning off” of active meso-domains driven by rearrangement of filler clusters. Thermal recovery of specimens implies that the parameters of the quasi-Gaussian distribution return to their initial values, but do not reach them even after recovery for  $t_a = 24$  h.

## **Acknowledgement**

We would like to express our gratitude to Dr. K. Fuller (TARRC, UK) for providing us with rubber specimens. Stimulating discussions with Profs. N. Aksel, A. Boukamel and S. Reese are gratefully acknowledged.

## References

- Aksel, N., Hübner, Ch., 1996. The influence of dewetting in filled elastomers on the changes of their mechanical properties. *Arch. Appl. Mech.* 66, 231–241.
- Bergström, J.S., Boyce, M.C., 1998. Constitutive modelling of the large strain time-dependent behavior of elastomers. *J. Mech. Phys. Solids* 46, 931–954.
- Bueche, F., 1960. Molecular basis for the Mullins' effect. *J. Appl. Polym. Sci.* 4, 107–114.
- Bueche, F., 1961. Mullins' effect and rubber–filler interaction. *J. Appl. Polym. Sci.* 5, 271–281.
- Clarke, S.M., Elias, F., Terentjev, E.M., 2000. Ageing of natural rubber under stress. *Eur. Phys. J. E* 2, 335–341.
- Dannenbergh, E.M., 1975. The effects of surface chemical interactions on the properties of filler-reinforced rubbers. *Rubber Chem. Technol.* 48, 410–444.
- Desmorat, R., Cartournet, S., 2001. Thermodynamics modelling of internal friction and hysteresis of elastomers. In: Besdo, D., Schuster, R.H., Ihlemann, J. (Eds.), *Constitutive Models for Rubber II*. Swets and Zeitlinger, Lisse, pp. 37–43.
- Doi, M., Edwards, S.F., 1986. *The Theory of Polymer Dynamics*. Clarendon Press, Oxford.
- Drozdov, A.D., 1996. *Finite Elasticity and Viscoelasticity*. World Scientific, Singapore.
- Drozdov, A.D., 2001. A tube concept in finite viscoelasticity of rubbers. In: Besdo, D.; Schuster, R.H.; Ihlemann, J. (Eds.), *Constitutive Models for Rubber II*. Swets and Zeitlinger, Lisse, pp. 93–104.
- Drozdov, A.D., Dorfmann, A., 2001. Finite viscoelasticity of filled rubbers: the effects of pre-loading and thermal recovery. *cond-mat/0110269*.
- Everaers, R., 1998. Constrained fluctuation theories of rubber elasticity: general results and an exactly solvable model. *Eur. Phys. J. B* 4, 341–350.
- Govindjee, S., Simo, J.C., 1992. Mullins' effect and the strain amplitude dependence of the storage modulus. *Int. J. Solids Structures* 29, 1737–1751.
- Green, M.S., Tobolsky, A.V., 1946. A new approach to the theory of relaxing polymeric media. *J. Chem. Phys.* 14, 80–92.
- Ha, K., Schapery, R.A., 1998. A three-dimensional viscoelastic constitutive model for particulate composites with growing damage and its experimental validation. *Int. J. Solids Struct.* 35, 3497–3517.
- Hansen, D.E., 2000. A mesoscale strength model for silica-filled polydimethylsiloxane based on atomic forces obtained from molecular dynamics simulations. *J. Chem. Phys.* 113, 7656–7662.
- Haupt, P., 2000. *Continuum Mechanics and Theory of Materials*. Springer-Verlag, Berlin.
- Haupt, P., Sedlan, K., 2001. Viscoplasticity of elastomeric materials: experimental facts and constitutive modelling. *Arch. Appl. Mech.* 71, 89–109.
- Häusler, K., Sayir, M.B., 1995. Nonlinear viscoelastic response of carbon black reinforced rubber derived from moderately large deformations in torsion. *J. Mech. Phys. Solids* 43, 295–318.

- Herman, M.F., 2001. A length scale dependent model for stress relaxation in polymer melts. *Macromolecules* 34, 4580–4590.
- Holzappel, G., Simo, J., 1996. A new viscoelastic constitutive model for continuous media at finite thermomechanical changes. *Int. J. Solids Struct.* 33, 3019–3034.
- Jäger; K.-M., McQueen, D.H., 2001. Fractal agglomerates and electric conductivity in carbon black polymer composites. *Polymer* 42, 9575–9581.
- Johnson, A.R., Stacer, R.G., 1993. Rubber viscoelasticity using the physically constrained system's stretches as internal variables. *Rubber Chem. Technol.* 66, 567–577.
- Johnson, A.R., Quigley, J., Freese, C.E., 1995. A viscohyperelastic finite element model for rubber. *Comput. Methods Appl. Mech. Engng.* 127, 163–180.
- Kaliske, M., Rothert, H., 1998. Constitutive approach to rate-independent properties of filled elastomers. *Int. J. Solids Structures* 35, 2057–2071.
- Karasek, L., Sumita, M., 1996. Characterization of dispersion state of filler and polymer–filler interactions in rubber–carbon black composites. *J. Mater. Sci.* 31, 281–289.
- Leblanc, J.L., Cartault, M., 2001. Advanced torsional dynamic methods to study the morphology of uncured filled rubber compounds. *J. Appl. Polym. Sci.* 80, 2093–2104.
- Liang, J.Z., Li, R.K.Y., Tjong, S.C., 1999. Effects of glass bead content and surface treatment on viscoelasticity of filled polypropylene/elastomer hybrid composites. *Polym. Int.* 48, 1068–1072.
- Lion, A., 1996. A constitutive model for carbon black filled rubber: experimental investigations and mathematical representation. *Continuum Mech. Thermodyn.* 8, 153–169.
- Lion, A., 1997. On the large deformation behavior of reinforced rubber at different temperatures. *J. Mech. Phys. Solids* 45, 1805–1834.
- Lion, A., 1998. Thixotropic behaviour of rubber under dynamic loading histories: experiments and theory. *J. Mech. Phys. Solids* 46, 895–930.
- Lulei, F., Miehe, C., 2001. A physically–based constitutive model for finite viscoelastic deformations in rubbery polymers based on a directly evaluated micro–macro–transition. In: Besdo, D., Schuster, R.H., Ihlemann, J. (Eds.), *Constitutive Models for Rubber II*. Swets and Zeitlinger, Lisse, pp. 117–125.
- Miehe, C., 1995. Entropic thermo-elasticity at finite strains: aspects of the formulation and numerical implementation. *Comp. Meth. Appl. Mech. Engng.* 120, 243–269.
- Miehe, C., Keck, J., 2000. Superimposed finite elastic-viscoelastic-plastoelastic stress response with damage in filled rubbery polymers. Experiments, modelling and algorithmic implementation. *J. Mech. Phys. Solids* 48, 323–365.
- Phan-Thien, N., Tanner, R.L., 1977. A new constitutive equation derived from network theory. *J. Non-Newtonian Fluid Mech.* 2, 353–365.
- Phan-Thien, N., 1978. A nonlinear network viscoelastic model. *J. Rheol.* 22, 259–283.
- Reese, S., Govindjee, S., 1998. Theoretical and numerical aspects in the thermo-viscoelastic material behaviour of rubber-like polymers. *Mech. Time-Dependent Mater.* 1, 357–396.
- Septanika, E.G., Ernst, L.J., 1998. Application of the network alteration theory for modeling the time-dependent constitutive behaviour of rubbers. 1. General theory. *Mech.*

Mater. 30, 253–263. 2. Further evaluation of the general theory and experimental verification. Mech. Mater. 30, 265–273.

Spathis, G., 1997. Non-linear constitutive equations for viscoelastic behaviour of elastomers at large deformations. Polym. Gels Networks 5, 55–68.

Treloar, L.R.G., 1975. The Physics of Rubber Elasticity. Clarendon Press, Oxford.

Wu, J.-D., Liechti, K.M., 2000. Multiaxial and time dependent behavior of a filled rubber. Mech. Time-Dependent Mater. 4, 293–331.

## List of figures

1. The dimensionless ratio  $R$  versus time  $t$  s in a relaxation test with the elongation ratio  $\lambda$  (virgin specimens). Circles: experimental data. Solid lines: results of numerical simulation
2. The dimensionless ratio  $R$  versus time  $t$  s in a relaxation test with the elongation ratio  $\lambda$  (pre-loaded specimens). Circles: experimental data. Solid lines: results of numerical simulation
3. The dimensionless ratio  $R$  versus time  $t$  s in a relaxation test with the elongation ratio  $\lambda$  (the specimens after recovery). Circles: experimental data. Solid lines: results of numerical simulation
4. The average potential energy of a meso-domain  $\langle\omega\rangle$  versus the first invariant  $I_1$  of the Cauchy deformation tensor. Symbols: treatment of observations. Unfilled circles: virgin specimens; filled circles: the specimens after pre-loading; asterisks: the specimens after recovery. Solid lines: approximation of the experimental data by Eq. (76)
5. The standard deviation of potential energies  $\sigma$  versus the first invariant  $I_1$  of the Cauchy deformation tensor. Symbols: treatment of observations. Unfilled circles: virgin specimens; filled circles: the specimens after pre-loading; asterisks: the specimens after recovery. Solid lines: approximation of the experimental data by Eq. (76)
6. The dimensionless ratio  $a$  versus the first invariant  $I_1$  of the Cauchy deformation tensor. Symbols: treatment of observations. Unfilled circles: virgin specimens; filled circles: the specimens after pre-loading; asterisks: the specimens after recovery. Solid lines: approximation of the experimental data by Eq. (79)
7. The dimensionless parameter  $\zeta$  versus the first invariant  $I_1$  of the Cauchy deformation tensor. Symbols: treatment of observations. Unfilled circles: virgin specimens; filled circles: the specimens after pre-loading; asterisks: the specimens after recovery. Solid lines: approximation of the experimental data by Eq. (80)

**Table 1:** Chemical composition of compound EDS-16 (phr by weight)

Formulation	Content
Natural rubber	100
Zinc oxide	5
Stearic acid	2
Carbon black (N330)	45
Process oil	4.5
Antidegradant(HPPD)	3
Antiozonant wax	2
Accelerator (CBS)	0.6
Sulphur	2.5

**Table 2:** Adjustable parameters of the model

Specimens	$\omega_0$	$\omega_1$	$\sigma_0$	$\sigma_1$	$a_0$	$a_1$	$\zeta_0$	$\zeta_1$
Virgin	5.1983	0.1157	3.8634	0.0346	0.3445	0.0312	0.7955	-0.0148
Preloaded	4.5786	0.1946	2.1424	0.1204	0.1452	0.0204	0.4755	0.0038
Recovered	5.0617	0.1488	3.3707	0.0189	0.3015	0.0270	0.6433	-0.0100

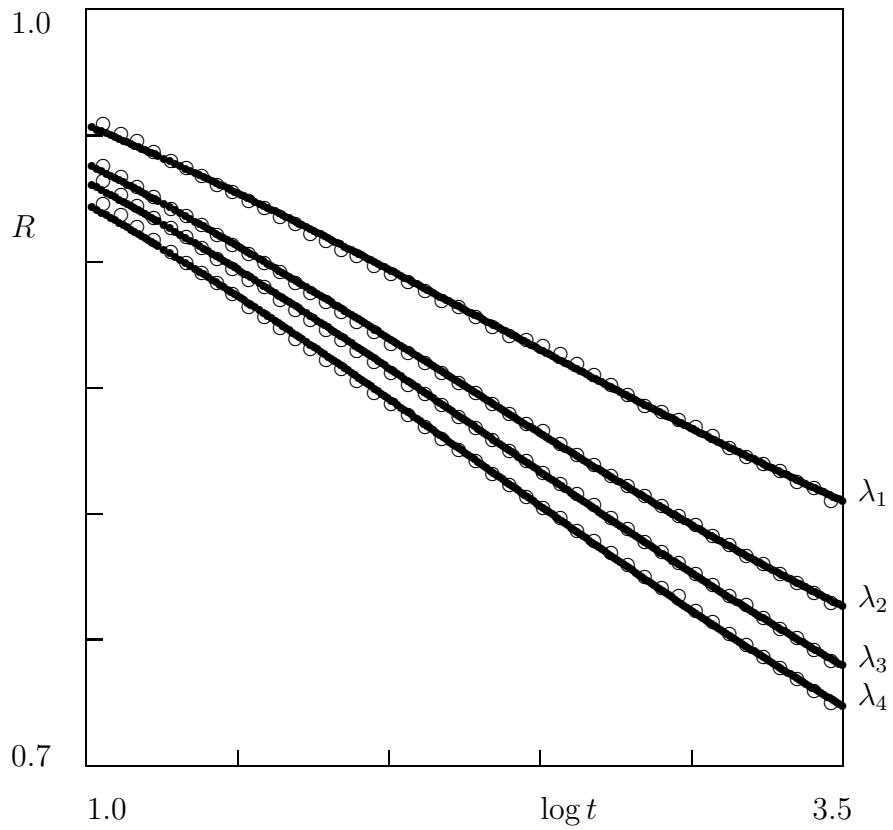


Figure 1: The dimensionless ratio  $R$  versus time  $t$  s in a relaxation test with the elongation ratio  $\lambda$  (virgin specimens). Circles: experimental data. Solid lines: results of numerical simulation

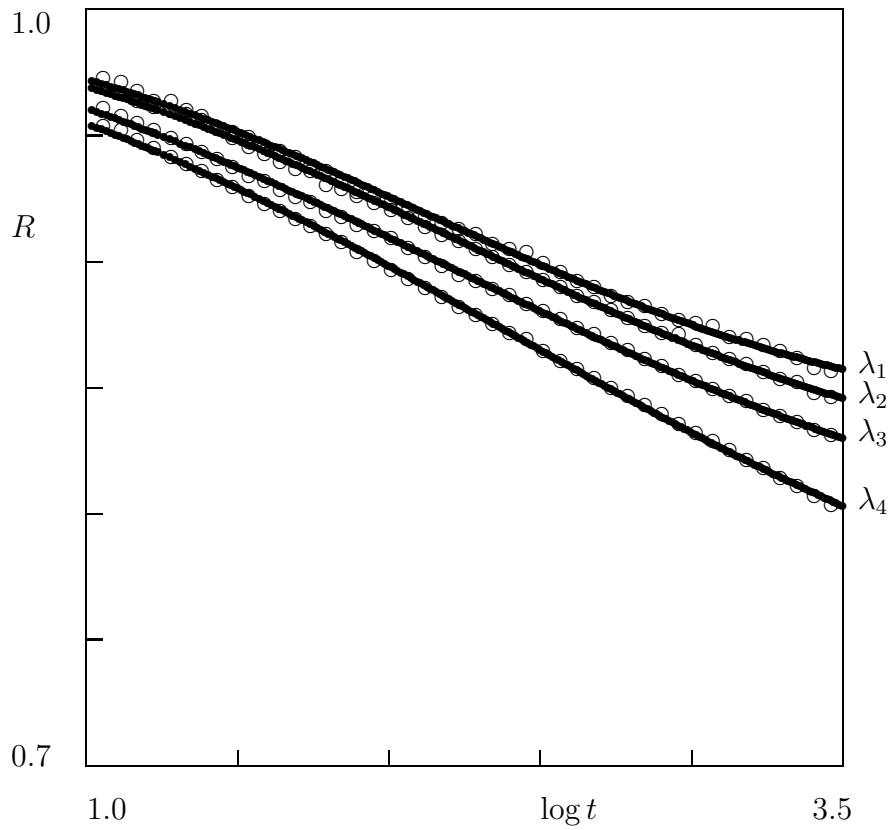


Figure 2: The dimensionless ratio  $R$  versus time  $t$  s in a relaxation test with the elongation ratio  $\lambda$  (pre-loaded specimens). Circles: experimental data. Solid lines: results of numerical simulation

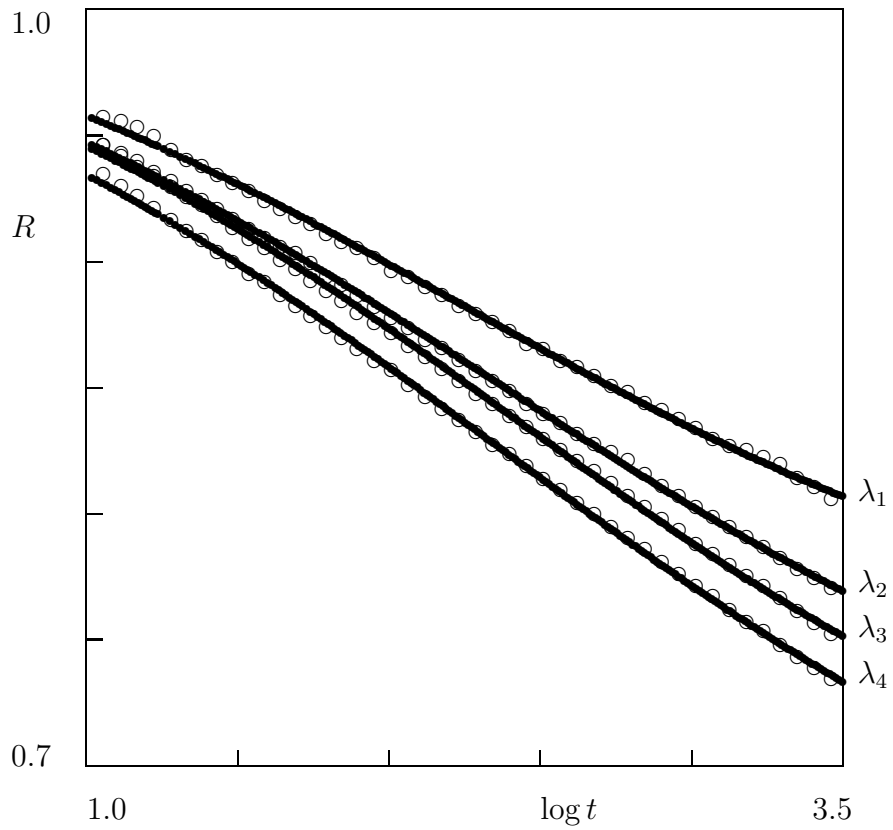


Figure 3: The dimensionless ratio  $R$  versus time  $t$  s in a relaxation test with the elongation ratio  $\lambda$  (the specimens after recovery). Circles: experimental data. Solid lines: results of numerical simulation

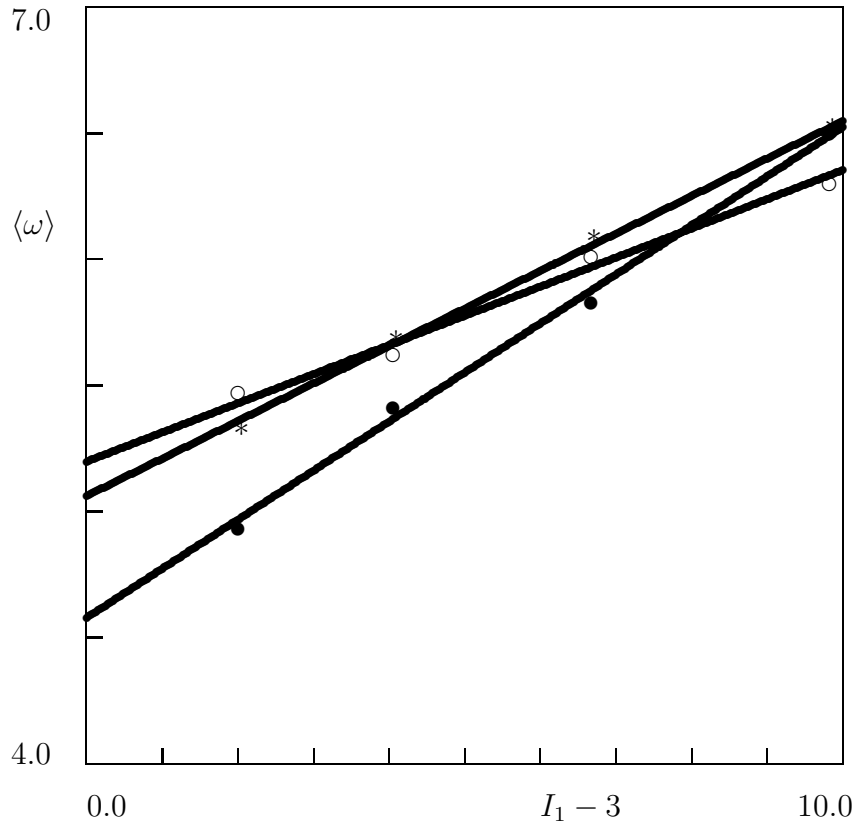


Figure 4: The average potential energy of a meso-domain  $\langle \omega \rangle$  versus the first invariant  $I_1$  of the Cauchy deformation tensor. Symbols: treatment of observations. Unfilled circles: virgin specimens; filled circles: the specimens after pre-loading; asterisks: the specimens after recovery. Solid lines: approximation of the experimental data by Eq. (76)

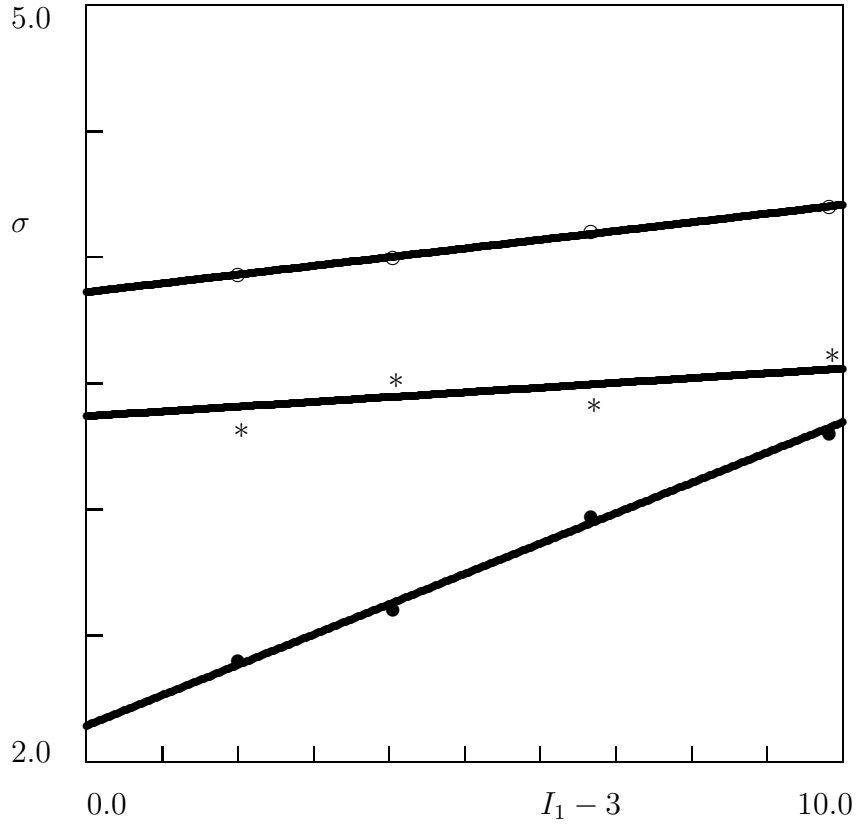


Figure 5: The standard deviation of potential energies  $\sigma$  versus the first invariant  $I_1$  of the Cauchy deformation tensor. Symbols: treatment of observations. Unfilled circles: virgin specimens; filled circles: the specimens after pre-loading; asterisks: the specimens after recovery. Solid lines: approximation of the experimental data by Eq. (76)

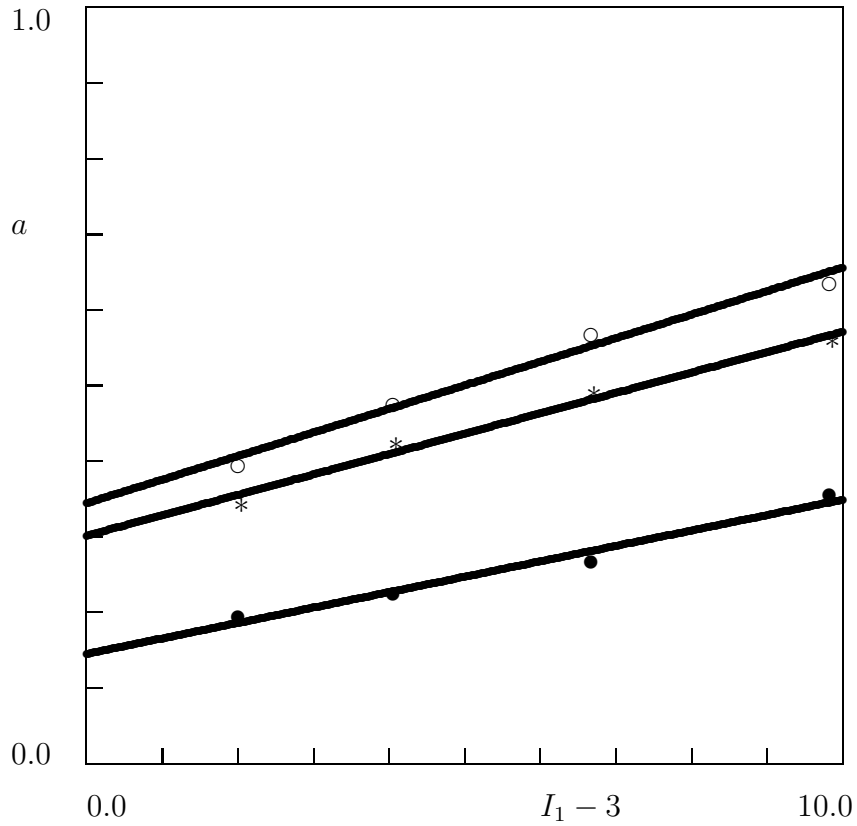


Figure 6: The dimensionless ratio  $a$  versus the first invariant  $I_1$  of the Cauchy deformation tensor. Symbols: treatment of observations. Unfilled circles: virgin specimens; filled circles: the specimens after pre-loading; asterisks: the specimens after recovery. Solid lines: approximation of the experimental data by Eq. (79)

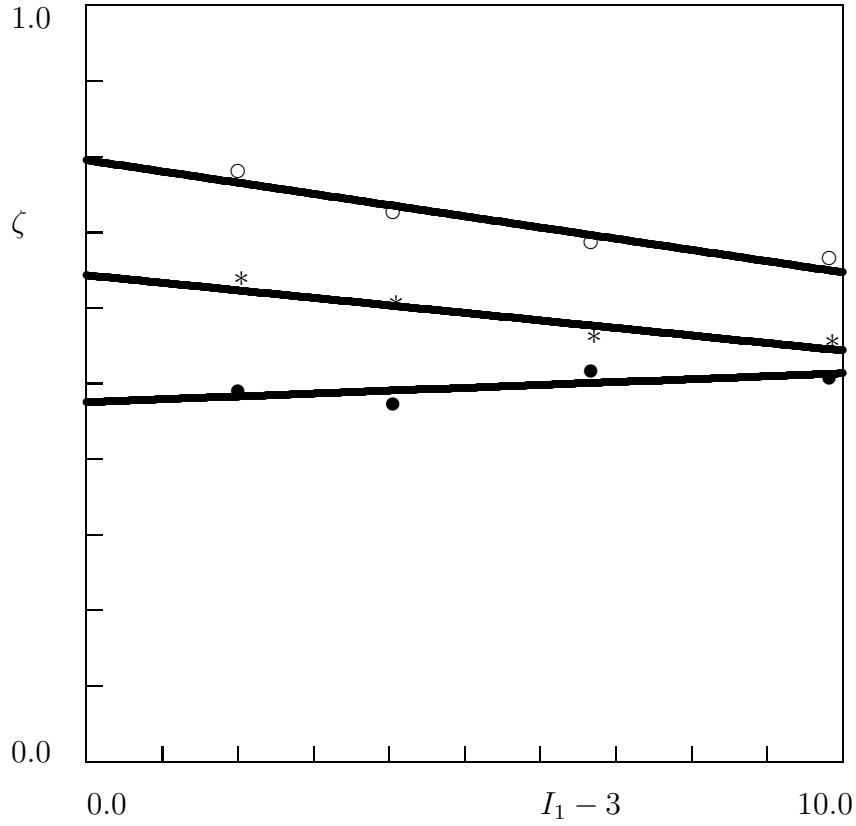


Figure 7: The dimensionless parameter  $\zeta$  versus the first invariant  $I_1$  of the Cauchy deformation tensor. Symbols: treatment of observations. Unfilled circles: virgin specimens; filled circles: the specimens after pre-loading; asterisks: the specimens after recovery. Solid lines: approximation of the experimental data by Eq. (80)